

석사학위논문
Master's Thesis

자동 용접 로봇을 위한
비전 기반 실시간 용접선 검출 기법

Vision-based Real-time Welding Line
Detection Algorithms for Automatic Welding Robot

2018

조정석 (曹正石 Cho, Jung-seok)

한국과학기술원

Korea Advanced Institute of Science and Technology

석사학위논문

자동 용접 로봇을 위한
비전 기반 실시간 용접선 검출 기법

2018

조정석

한국과학기술원

조천식녹색교통대학원

자동 용접 로봇을 위한
비전 기반 실시간 용접선 검출 기법

조 정 석

위 논문은 한국과학기술원 석사학위논문으로
학위논문 심사위원회의 심사를 통과하였음

2017년 12월 05일

심사위원장 김 경 수 (인)

심 사 위 원 장 인 권 (인)

심 사 위 원 하 동 수 (인)

Vision-based Real-time Welding Line Detection Algorithms for Automatic Welding Robot

Jung-seok Cho

Advisor: Kyung-soo Kim

A dissertation submitted to the faculty of
Korea Advanced Institute of Science and Technology in
partial fulfillment of the requirements for the degree of
Master of Science in Green Transportation

Daejeon, Korea
December 05, 2017

Approved by

Kyung-soo Kim
Dean of The Cho Chun Shik Graduate School of Green Transportation

The study was conducted in accordance with Code of Research Ethics¹.

¹ Declaration of Ethical Conduct in Research: I, as a graduate student of Korea Advanced Institute of Science and Technology, hereby declare that I have not committed any act that may damage the credibility of my research. This includes, but is not limited to, falsification, thesis written by someone else, distortion of research findings, and plagiarism. I confirm that my thesis contains honest conclusions based on my own careful research under the guidance of my advisor.

MGT

20154554

조정석. 자동 용접 로봇을 위한 비전 기반 실시간 용접선 검출 기법 . 조천식녹색교통대학원 . 2018년. 83+iv 쪽. 지도교수: 김경수. (영문 논문)
Jung-seok Cho. Vision-based Real-time Welding Line Detection Algorithms for Automatic Welding Robot . The Cho Chun Shik Graduate School of Green Transportation . 2018. 83+iv pages. Advisor: Kyung-soo Kim. (Text in English)

초 록

건축, 조선, 자동차 등 중공업 제조 산업에서 용접 기술은 제조된 제품의 품질을 결정하는 중요한 역할을 한다. 특히, 조선업의 경우 철재 용접이 전체 작업량의 상당히 많은 부분을 차지한다. 생산성 향상을 위해 용접의 자동화에 대한 연구는 산업과 학계에서 중요한 분야 중 하나로 인식되어 왔다. 기존 연구에서 변위 센서를 이용하여 용접 로봇이 용접면을 수직으로 따라가는 정도의 간단한 자동화는 이루어졌지만, 정확한 용접선을 따라가기 위해서는 여전히 사용자의 모니터링 하에서 제어되어야 하는 결정적 단점을 가지고 있다. 또한, 컴퓨터 비전을 이용하여 용접선을 검출하는 기존 연구들은 용접 시 발생하는 아크(arc)에 의해 영상의 품질이 크게 저하되어 실시간으로 용접선을 추정하는 방법에 대한 연구가 적고, 이에 대해 다룬 연구라도 실시간으로 다양한 철재 모형을 고려하지 못하고 용접선을 높은 정확도로 추정하지는 못하고 있다. 따라서 본 연구에서는 광학 및 비전을 이용하여 이러한 단점들을 해결할 수 있는 방안에 대해서 제시한다.

핵심 낱 말 광학 기반 시스템, 비전 기반 시스템, 실시간 용접선 추적, 자동 용접 로봇 비전 센서

Abstract

In heavy manufacturing industries, such as construction, shipbuilding, and automobile, the welding technology plays an important role in determining the quality of manufactured products. Especially in the case of the shipbuilding, steel welding accounts for a considerable portion of the overall workload. In order to improve productivity, research on automation of welding processes has been recognized as one of the important fields in industries and academia. Recently, a simple automation of the welding robot perpendicularly following the welding surface using a displacement sensor has been developed, but it still has a considerable disadvantage that it must be monitored by the user to follow the exact weld line. In addition, existing technologies to detect the weld line using computer vision have been limited to estimating the weld line in real time because the quality of the image is deteriorated due to the arc generated in the welding. To address the limitation, this study suggests an arc-insensitive optical system and a real-time processing algorithm using spectrum analysis and computer vision algorithms.

Keywords optical-based systems, vision-based systems, real-time seam tracking, automatic welding robots, vision sensors

Contents

Contents	i
List of Tables	iii
List of Figures	iv
Chapter 1. Introduction	1
1.1 Research Background	1
1.2 Related Works	3
1.2.1 Research of Optical Characteristics for Arc Quality In- spection During Welding	4
1.2.2 Research on Quality Verification after Welding	10
1.2.3 Research on Welding Line Detection	10
1.3 Research Objective	18
Chapter 2. Design Optical System	19
2.1 Spectroscopy[31, 32]	19
2.2 Welding Arc Spectrum Analysis	20
2.2.1 Configuration of the experimental equipment	20
2.2.2 Experimental Results	21
2.3 Process of Camera Selection	23
2.3.1 Determining Camera Absorption Wavelength	23
2.3.2 Determining Camera Model	24
2.4 Process of Optical Filter and Laser Selection	27
2.4.1 Principles and Terminology of Optical Filter[25]	27
2.4.2 Constraints and Selection of Optical Filter	31
2.4.3 Constraints and Selection of Laser	31
2.5 Experiments and Results	33
2.5.1 Experiment Configuration	33
2.5.2 Results	35
2.5.3 Conclusion	42
Chapter 3. Welding Line Detection	43
3.1 Background of Image Processing	43
3.1.1 Image Enhancement using Histogram Transformation	44
3.1.2 Image Enhancement using Spatial Filter	49
3.2 Background of Computer Vision[59]-[62]	53

3.2.1	Template Matching	53
3.3	Process of Welding Line Detection	54
3.3.1	Image Quality Enhancement	55
3.3.2	Welding Line Detection	58
3.4	Results	66
Chapter 4.	Conclusion and Future Works	71
4.1	Conclusion	71
4.2	Future works	71
	Bibliography	74
	사 사	81
	약 력	83

List of Tables

2.1	Power Ratio Result of Optical Systems	40
3.1	Welding line detection result	70

List of Figures

1.1	Worldwide LNG Demand	1
1.2	GTT Corp. LNG tank, HHI(Hyundai heavy industry LNG tank	3
1.3	Welding robot Mark 3(HHI)	3
1.4	Welding position according to welding position	4
1.5	GTAW welding principle	5
1.6	Images of the torch portion at different frequencies	6
1.7	In case of bad welding, images put through various image processing	8
1.8	Image of thermal camera according to welding process during welding	8
1.9	Signals change according to welding distance in normal and bad welding section	8
1.10	Changes in the distribution of spectra when welding according to current	9
1.11	Spectral distribution during welding in air and water	9
1.12	A laser formed differently depending on the geometric characteristics	9
1.13	Outline of coordinate system of proposed seam detection system in [15]	11
1.14	Laser image used in [15]	12
1.15	Proposed detection method and 3D restoration result in [19]	12
1.16	Change of laser length according to height[17]	13
1.17	Hough transformation	14
1.18	Background detection using Hough transform[22]	15
1.19	Study of detecting weld line directly using Hough transform[22]	15
1.20	Study of detecting weld line directly using Hough transform[22]	16
2.1	Geometric factors that cause step differences	19
2.2	Configuration of experimental equipment for arc spectrum analysis	21
2.3	Results of welding arc spectrum analysis	22

2.4	Bloom-smear phenomenon	24
2.5	Spectral response graph of infrared camera	25
2.6	FL3-U3-20E4C-C Camera's Spectral response	25
2.7	FL3-U3-20E4C-C camera model of Point gray	25
2.8	Estimated spectral response graph	26
2.9	Principle of optical filter	28
2.10	The graph for illustrate optical filters terminology	29
2.11	Filter spectrum response graph	30
2.12	Laser irradiation angle	32
2.13	Results obtained by reducing laser width	32
2.14	Welding robot step file	34
2.15	Welding robot shape after attaching optical system	35
2.16	Comparing the results before and after attaching the optical system	36
2.17	Comparison of 905nm and 980nm laser system	37
2.18	Result of 905nm optical system	39
2.19	Result of 980nm optical system	40
3.1	Image histogram	44
3.2	Histogram results of images with different brightness	44
3.3	Two images with different brightness of the same subject	45
3.4	Gamma function	46
3.5	Gamma correction result	47
3.6	Histogram transformation	48
3.7	2D convolution	50
3.8	Laplacian kernel	51
3.9	Kernels and results	52
3.10	Template matching	54

3.11	Welding line detection overall process flow	54
3.12	ROI extraction	55
3.13	Bilateral filtering	56
3.14	Otsu's binarization	57
3.15	Results of image enhancement	57
3.16	Laser geometry	58
3.17	Binarization image	58
3.18	Template matching	59
3.19	Symmetric padding	60
3.20	template matching with modified kernel	61
3.21	template matching process and result of image	62
3.22	probability density fuction	63
3.23	Feature point map generation process	63
3.24	Outlier image	65
3.25	Outlier dection	66
3.26	Summary of outlier detection	66
3.27	Welding line detection result 1	68
3.28	Welding line detection result 2	69
4.1	Vanishing view point problems	73

Chapter 1. Introduction

1.1 Research Background

Due to the global economic depression, the size of the merchant marine market is on the decline. In addition, the commercial shipbuilding market is relatively labor intensive due to its relatively low technology level. Therefore, the market of the shipbuilding industry, which is the main industry of domestic shipbuilding industry, is being affected by the expansion of the shipbuilding production facilities in countries with low labor costs such as China recently. Therefore, the Korean shipbuilding industry is inevitably expanding into a market that requires more advanced technology, except for the merchant ship market, which requires a great deal of expertise. As a solution to this situation, LNG shipbuilding orders are increasing rapidly due to the recent increase in LNG demand. Domestic and foreign companies are busy making efforts to secure orders.

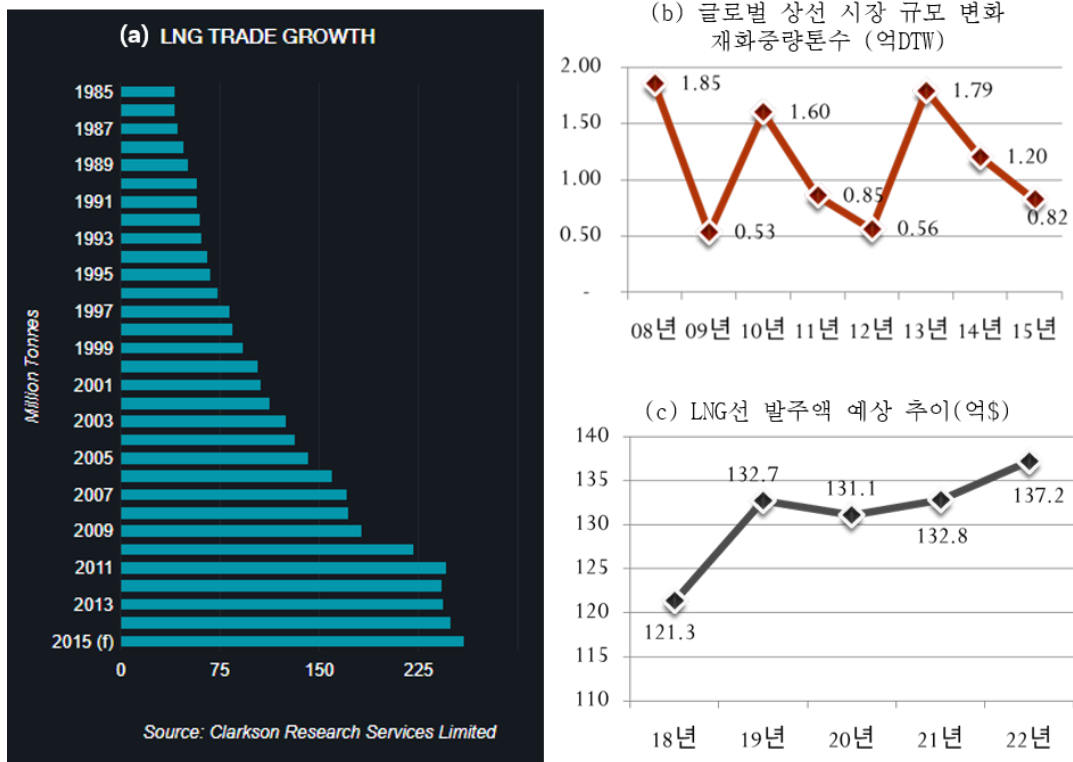


Figure 1.1: (a): Worldwide LNG Demand[tonne] Demand histogram, (b): Changes in global merchant marine market size, (c): Order forecast for LNG carriers

As of 2014, the total number of orders for world LNG carriers is 66 units. Among them, orders for domestic is about 76% of total orders, in 2013, 28 orders (61%) out of 46 orders in the world, and 61% of orders in 2012 (39 orders in 2012). LNG carrier orders are expected to rise sharply from the USD 12.1bn in 2017 to the USD 13.7bn in 2022. Currently, 70% of the total demand is built in Korea. In order to maintain this, it is very important to secure domestic source technologies in order to dominate the shipbuilding industry such as China.

One of the most important parts of LNG shipbuilding is the tank containing the LNG cargo hold as shown in the Figure 1.2 (a). The LNG cargo holds a liquefied natural gas tank at 163 °C. The inner wall is made of stainless steel and the outer wall is made of polyurethane. In the case of Hyundai Heavy Industries, GTT is paying royalties of 5 % on the basis of its source technology, which is about 10 billion won per square meter.

In order to lessen the burden on these royalties, domestic companies have secured their own cargo hold technology and Hyundai Heavy Industries is developing technology to make cargo holds with its own technology. As shown in Figure 1.2 (b), the steel was made of double barrier, and the insulation and strength were excellent, and the LNG vaporization rate was reduced by 10 % compared to GTT.

Most important parts of making a membrane LNG tanks is the accuracy of the weld. Welding accuracy is an important factor that affects the overall insulation of the tanks, which is naturally related to the rate of vaporization. Therefore, domestic and foreign companies are investing a lot in the welding process, and a welding robot (Mark III) capable of welding with the curved surface of steel following the Figure 1.3.

A total of 54 km of weld line must be welded to create one membrane LNG tank. Considering that the Mark III welding speed is 300mm/min, it takes 3000 hours to use one Mark III to create one tank. And also there is no function to follow the weld line in real time so it is required to monitor and controlled. For long time and welding, it is necessary to be in an inconvenient position depending on the position of the welded line, such as lifting the head, bowing the waist, or bending the knee. It is a work involving physical fatigue, especially in the eye due to strong arcs. Because of the inefficiency and

the risk of the operator, it is necessary to develop a welding robot of a level capable of monitoring the worker intermittently by following the welding line instead of the welding robot which always depends on the monitoring of the welding person.

Therefore, in this study, we propose a method to detect the weld line by developing vision-optics based system, which is the core part of the development of welding robots.

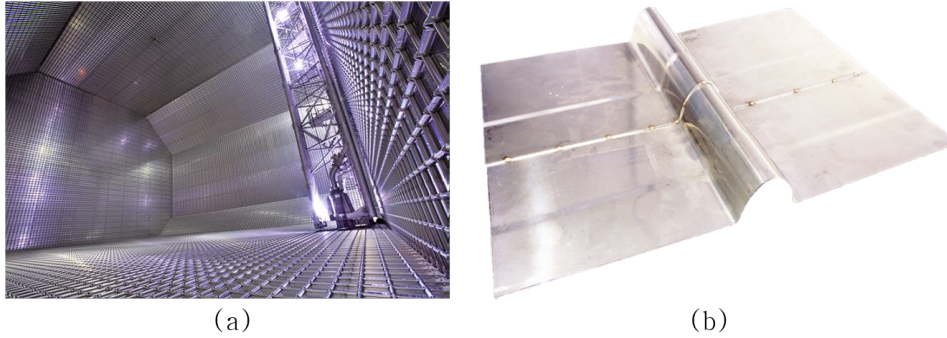


Figure 1.2: GTT Corp. LNG tank, HHI(Hyundai heavy industry LNG tank, (a): Existing LNG holdings produced by GTT in France, (b): Corrugated plate for LNG cargo hold barriers manufactured by Hyundai Heavy Industries

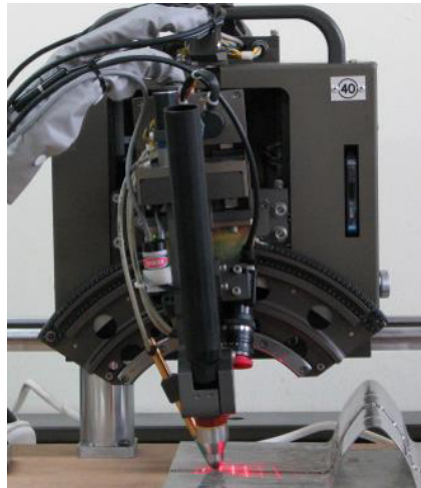


Figure 1.3: Welding Robot Mark III(HHI)

1.2 Related Works

As I mention the importance of welding in the shipbuilding industry mentioned above, research on welding has been proceeding actively. In order to improve the welding quality during welding, research has been carried out to find a new welding method by approaching chemical materials in a way that different



Figure 1.4: Welding position according to welding position

materials are reacted for welding. In order to improve quality and stability of welding, shielding Gas is also being studied. Research is also underway to find the most optimal chemical structure compatible with the steel to be welded.

In addition to the studies on the chemical content listed above, there are a lot of studies for automation of welding mainly on mechanical and electronic elements. In this section, we present a case study of optical and computer vision technology used in this paper for automatic welding.

Mainly used fields can be abbreviated as weld quality inspection or weld line detection. There are some products that are actually commercialized with this. Welding quality inspection consists of (1) analysis of the characteristics of arc light or image processing technology from the welding torch, (2) research to verify the quality of the welded parts by using the image processing and computer vision after irradiating the laser of the welding line of the welded steel. Lastly, And 3) research that detects weld lines to be welded during welding using image processing and computer vision. In this section, we present the representative papers on the three cases listed above and discuss its limitations.

1.2.1 Research of Optical Characteristics for Arc Quality Inspection During Welding

The figure 1.5 is an illustration that explains the overall description of the welding process. In brief, welding is a process in which an electrode injecting electrons serves as a negative electrode, and a welding material acts as a positive electrode. And the heat of the oxidation-reduction reaction. During this process, a plasma phenomenon occurs and high temperature heat is generated. As a result of this

heat, the steel can be melted and welded. During this process, a shielding gas is generated to prevent interference with the surrounding gas.

The arc generated during welding consists of complicated modeling of the causes of welding such as temperature, voltage, and short-circuit time, and they are modeled and controlled differently by each welding process. [2]-[4]. The quality inspection of the arc, which is the result of this complex process, is considered very important because it is an important parameter for evaluating the performance of welding in welding. [5]-[11] can be divided into direct inspection method [5], [6] and indirect inspection method [1], [5]-[11].

Direct inspection is done by measuring the arc modeling and the difference between the sensor values of the causes that generate the arc. However, the values corresponding to the electrical characteristics parameters are random and can vary widely. The paper [6] points out this point and discusses the need to avoid the deterministic method and to direct the stochastic method. Therefore, for the inspection of the arc, probability density distributions and class frequency distributions based on electrical characteristic parameters are defined, and the quality is checked using neural network learning with probability density distributions and frequency distributions according to various situations.

As the hardware has been able to guarantee real-time processing of spectrometers with high resolution to price, arc inspection using them has been newly proposed. In the paper [5] - [7], we point out the

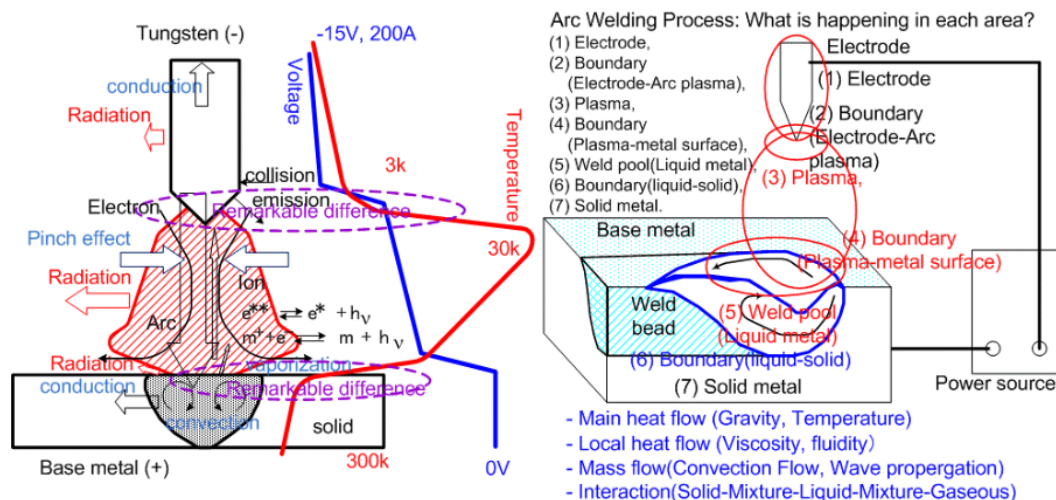


Figure 1.5: Gas Tungsten Arc Welding, GTAW welding principle[1]

limitations of the existing electrical property parameters and combine the frequency components and the arc modeling results spectroscopically to visually analyze the arc features It is suggesting. As the quality of the arc can be inspected by analyzing the frequency using the spectroscope, the research has been carried out by indirectly examining the arc such as spectroscopy and image instead of using the electrical characteristic parameter.

A typical reference for indirect inspection is [1]. In this paper, we propose a new method of image processing that uses 1) arc diffusion, 2) mean value, 3) median value, 4) maximum value, 5) 6) It is a very detailed technical report on standard deviation value analysis and 7) frequency analysis using spectroscopy.

In figure 1.6, a bandpass filter lens which can pass only a single frequency of the arc part generated in the welding of GTAW welding, to be.

The sensitivity of the image sensor is affected by the wavelength, and the normal CMOS and CCD based image sensors have the highest sensitivity in the range of 500-700nm. Sensitivity in wavelength bands of 400nm or less and 900nm or more is 1/4 or less of the visible light range.

In addition, since the reduction effect by the lens differs according to the wavelength, it is difficult to perform a clear analysis between single frequencies according to a clear frequency band. However, as shown in the figure, it can be understood that the information received by the image sensor depending

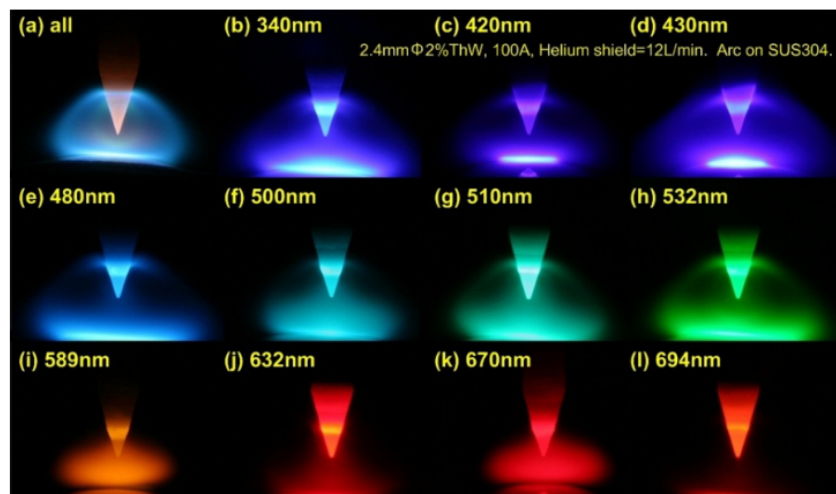


Figure 1.6: Images of the torch portion at different frequencies [1]

on the frequency component may be clearly different .

The picture 1.7 suggests that image processing algorithms can be used in various ways to detect sparks when poor welding occurs due to lack of protective gas or positive electrodes during welding, 1.8 indicates that the degree of diffusion of heat through the thermal imaging camera can be determined to distinguish the welding process. As such, in the 2010s, a number of methods for verifying the inspection of the arc through an indirect method have been proposed, and it is still actively in progress.

Another similar study is shown in [9]. As can be seen from the figure 1.9, it is possible to detect the defect of the welded state sufficiently as a result of several frequency components and neural network learning obtained through principal component analysis of the spectra obtained through the spectroscopy. It suggested that it can take a lot of computational gains. Plus, the frequency component detected by the principal component analysis as in the figure 1.10 suggests that it is independent of the welding strength controlled by the intensity of the current. In addition, the welding spectrum appears to be irrelevant not only to the intensity of the current but also to the surrounding environment, suggesting that the distribution of the spectrum is constant even under water in the paper [8]. This makes it possible to conclude that the frequency distribution is constant for light intensity variations(current) and noise(water), respectively.

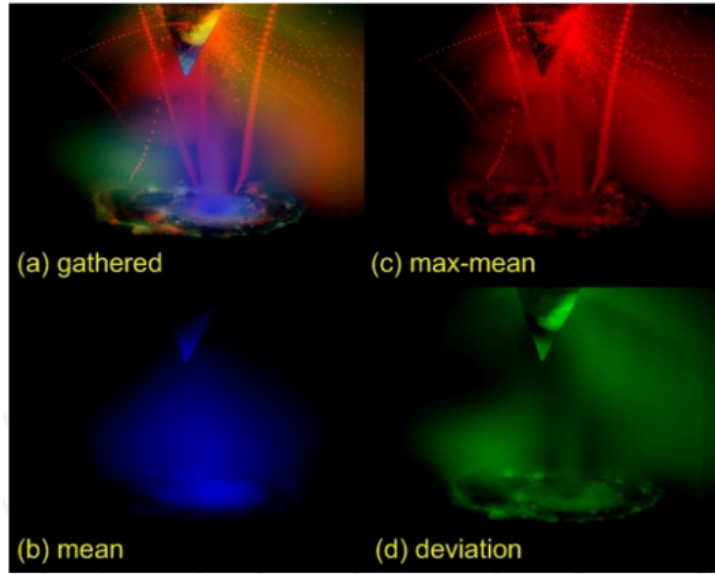


Figure 1.7: In case of bad welding, images put through various image processing [1]

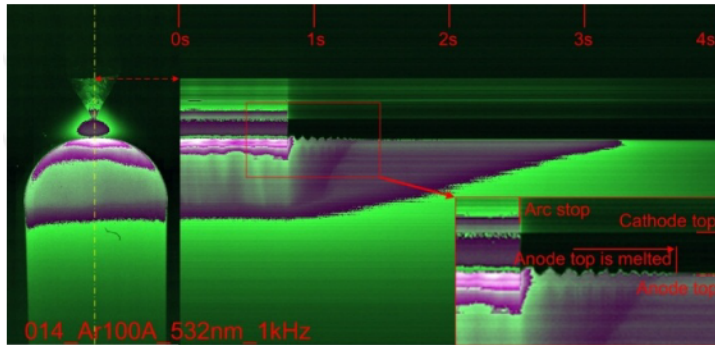


Figure 1.8: Image of thermal camera according to welding process during welding[1]

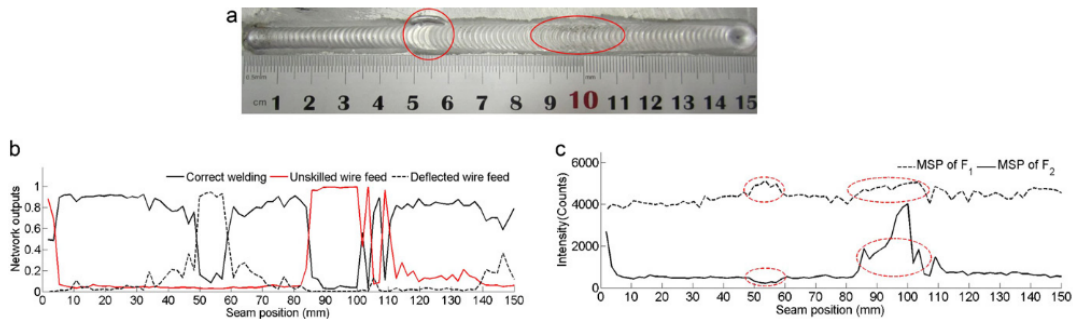


Figure 1.9: Signals change according to welding distance in normal and bad welding section, (a): Two sections obtained as a result of bad welding, (b): Output value of neural network learning, (c): Frequency intensity variation of two frequency components obtained by principal component analysis [9]

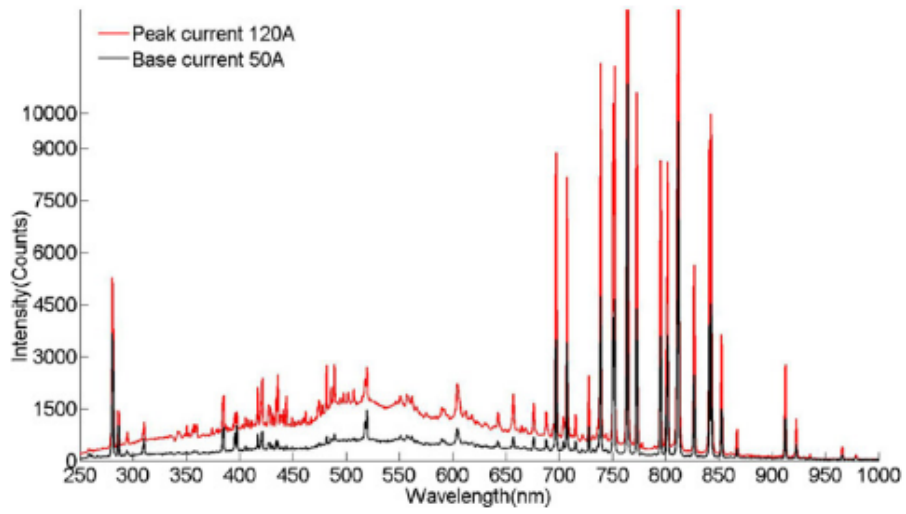


Figure 1.10: Changes in the distribution of spectra when welding according to current[9]

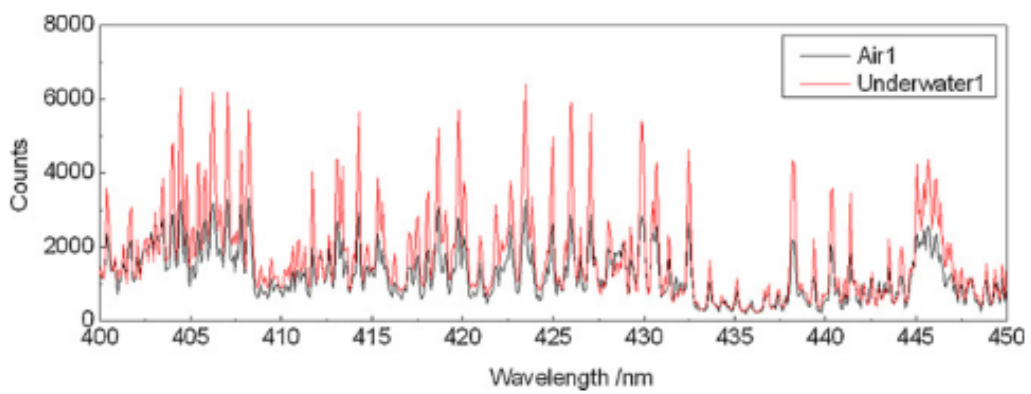


Figure 1.11: Spectral distribution during welding in air and water[8]

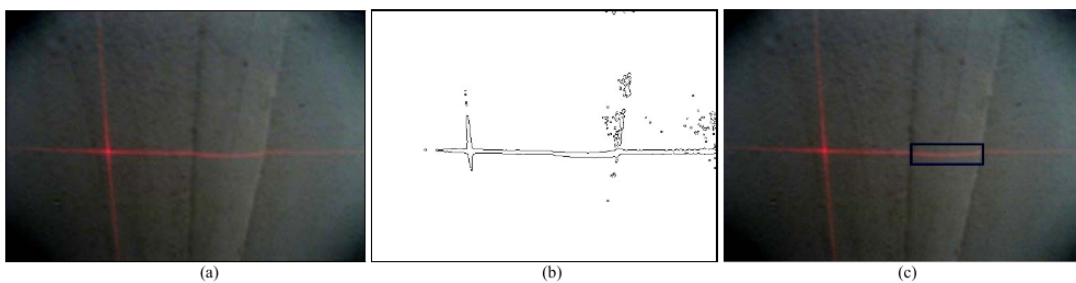


Figure 1.12: A laser formed differently depending on the geometric characteristics, (a): laser irradiation of welded steel, (b) binarization image obtained by image processing, (c) welding surface detection through hidden Markov model[12]

1.2.2 Research on Quality Verification after Welding

A study has also been carried out on the validity of the weld where the weld has been completed for the secondary inspection [12]-[14]. For the most part, non-destructive testing is performed using the laser, camera, etc. in order not to change the state after welding, and high-precision research has been conducted for special inspection equipment such as [12, 14], X-RAY. However, the performance of the hardware has improved these days and researchers have been actively conducted to verify the welding quality using a relatively inexpensive camera.

The paper [12] investigates the cross-shaped structure light and detects the geometric characteristics of welded and non-welded surfaces as shown in figure 1.12 and uses the hidden Markov model to extract the weld line robustly. According to this paper, it is suggested that using the geometric information of steel can sufficiently detect the welding surface by using the algorithm of computer vision.

Sensor fusion with data obtained using other sensors may be used to improve the uncertainty of the information acquired with the image information. In [14], the weld line is detected by fusing information read from the distance to the weld surface with information obtained from the image with a displacement sensor. In order to fuse through the obtained results, the optimal estimate is obtained by using the probability model of the prediction result and the estimation result.

The purpose of the discussion in subsection 1.2.1 are the same but differ in that they are done at the time of welding and after welding. Relatively it inaccurate during the welding process, but it is a preferred method in the industry to saves time. In industries that require precise welding, such as semiconductor equipment, researchers on post-weld quality verification are also underway in industries that require secondary inspection

1.2.3 Research on Welding Line Detection

It is the most relevant to the research to be presented in this paper and is one of the most active researches in recent years. If you use a laser, you can categorize it into two categories: [15] - [19] and [20] - [25]. It categorized whether use laser or not. In the case of using the laser, two steel materials to

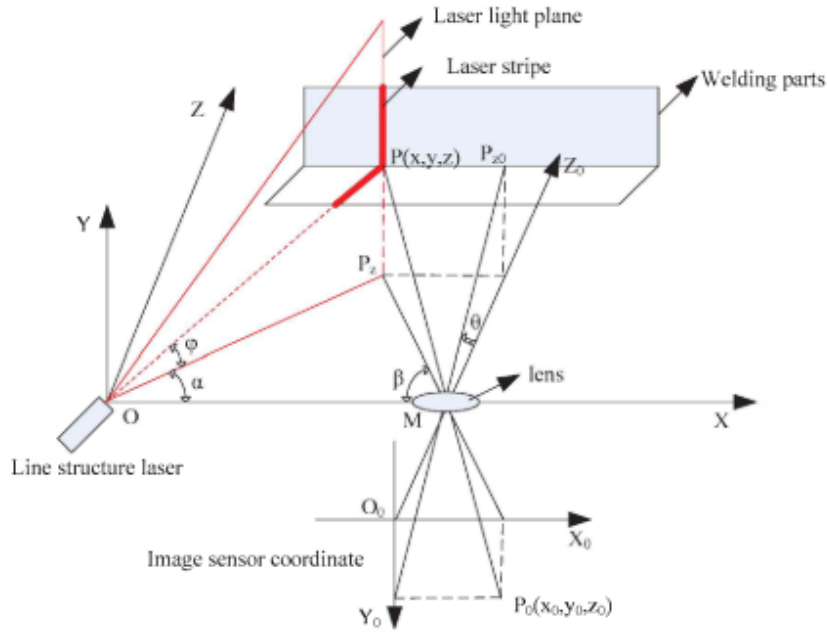


Figure 1.13: utline of coordinate system of proposed seam detection system in [15]

be welded overlap each other so it has clear geometric characteristics. On the contrary, when the laser is not used, it is usually used for welding a small steel on one steel.

As for the study using the laser, in [15], as shown in figure 1.13, two pieces of iron are inserted in the form of 'L' shape and the laser is irradiated there. Then the laser part viewed from the camera appears as picture 1.14. As can be seen from the figure 1.14, when two steel materials are connected in a manner having different geometric characteristics, distinguishable feature points can be found in the image, which is sufficiently accurate without the implementation of complex algorithms to detect welding line.

Among the researchers using the laser, [17], which is not used in welding but inspired much for this research. In [17], it is suggested that the length of the laser in the image varies according to the height when the laser is irradiated at a constant height as shown in the figure 1.16, and the 3D shape can be restored by using it. The idea of this study suggests that if there is a difference in the height of welded steel, there will be a difference in the image that can be distinguished by the height and angle of the laser.



Figure 1.14: Laser image used in [15]

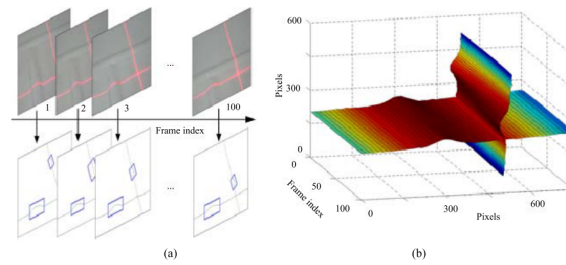


Figure 1.15: Proposed detection method and 3D restoration result in [19], (a): weld line detected in each frame, (b): visualization in three dimensions using it[19]

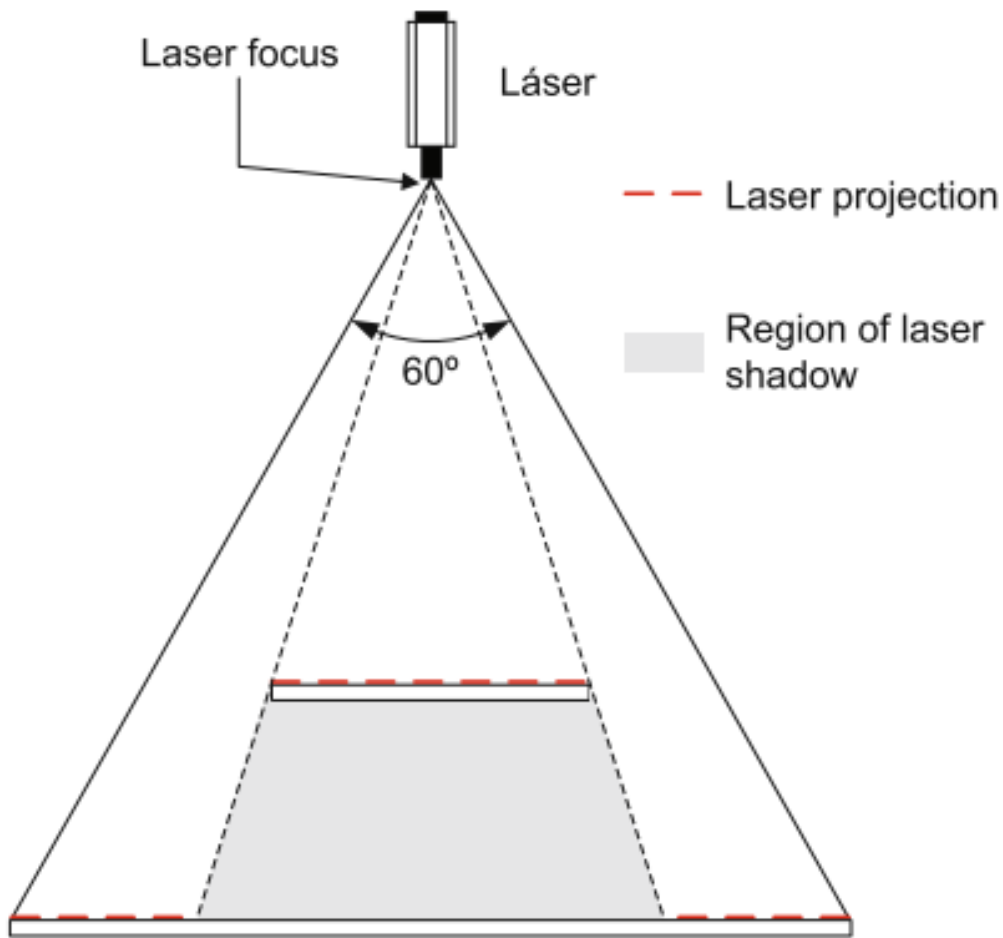


Figure 1.16: Change of laser length according to height[17]

The most commonly used method in non-laser studies is the Hough transform. The Hough transform transforms a Cartesian coordinate into a polar coordinate with the formula 1.1 and use the feature which obtained by span of an angle(θ) and a length(ρ). In Cartesian space, the point appears as a triangular function in the Hough space, and the line segment as a point. The time complexity of Hough transform is $O(A^{m-2})$. A is the size of image, m number of the estimated parameters. In the case of a straight line used for welding line detection, the number of parameters to be estimated is 3 and the amount of calculation is not so large. However, since the Hough transform finds the principal straight line component by voting the number of intersections of the trigonometric functions corresponding to each calculated pixel. If the pixel value is insufficient for the principal straight line component, finding a

straight line becomes difficult to detect[37].

$$\rho = x \cos \theta + y \sin \theta \quad (1.1)$$

Using this, it is possible to detect a line segment by using Hough transform [26] in the image, and [22, 24, 25]. [22] detected a line segment of steel through Hough transform as shown in figure 1.18. It is suggested that the ROI can be extracted through Hough transform and the remaining image can be removed, and as a result, the image interference such as noise outside the ROI can be reduced.

A study to directly detect the weld line using Hough transform is [24, 25]. [25] explains that it is useful in cases where there is severe noise around the line because the line segment is not clear as in the figure 1.19 (a). This is possible with the calculation of probability per pixel [27, 28]. The probability-based Hough transform increases the amount of computation in proportion to the size of the image compared with the existing Hough transform. This probability-based Hough transformation has a lot of computations, so there are many studies[29, 30] on the reduction of the computational complexity. Considering the implications for the computational complexity, the probability-based decision model on the pixel basis is not good in the industry that emphasizes real-time process.

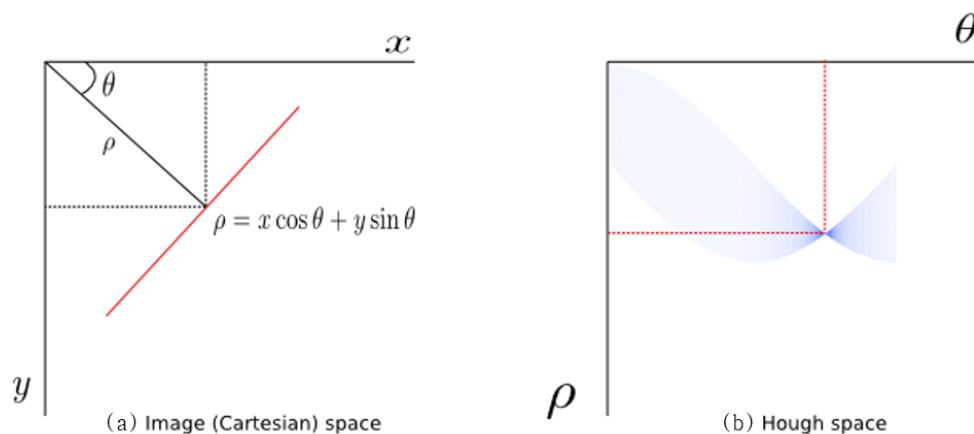


Figure 1.17: Hough transformation, (a): Cartesian space, (b): Hough space

The method of using and detecting Hough transform is mainly computed by pixel by pixel calculation [20], or by inserting a marker artificially, it makes it recognizable in the image and then detects the weld line[20]. Although there is an advantage in accuracy rather than Hough transformation, It Being studied

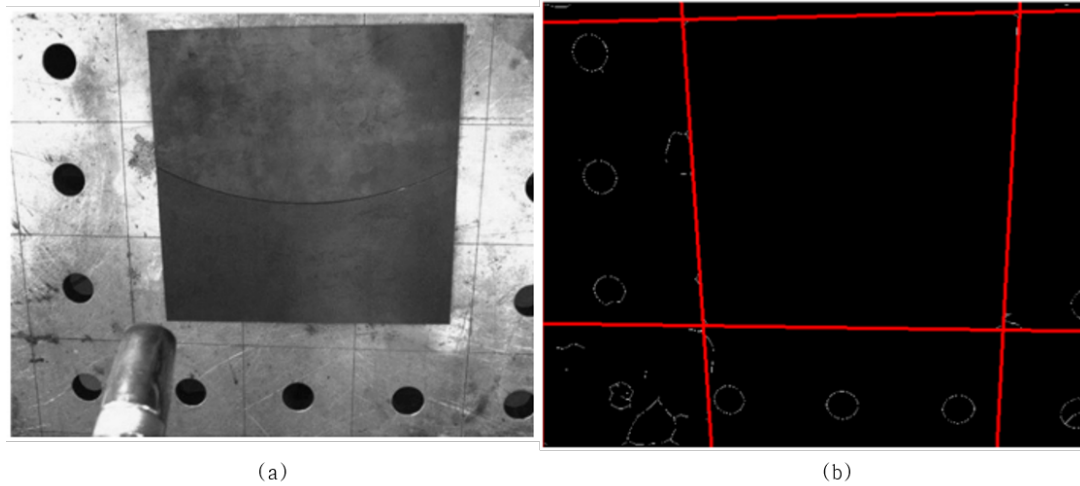


Figure 1.18: Background detection using Hough transform[22]

intermittently because the algorithm is not robust and artificial mark insertion is required. .

In order to find a single line segment, a pixel-by-pixel search approaches the assumption that there is a difference in contrast between the welding line and the other regions. Therefore, it is possible to extract the weld line by using the correlation between light and darkness of the weld line using image processing, suggests that the noise of the extracted edge can be removed by extracting one consistent contour line by computing all eight orientations that can move in the pixel as in the figure 1.20 (a). However, if it goes beyond the searching window, it may fall into the local minimum and may not detect it properly. In addition, it may fall into an infinite loop and cause serious danger in pixel unit calculation. Therefore, the method of detecting the welding line based on the pixel calculation requires a lot of effort in the image processing technique of performing thresholding according to the difference in contrast in

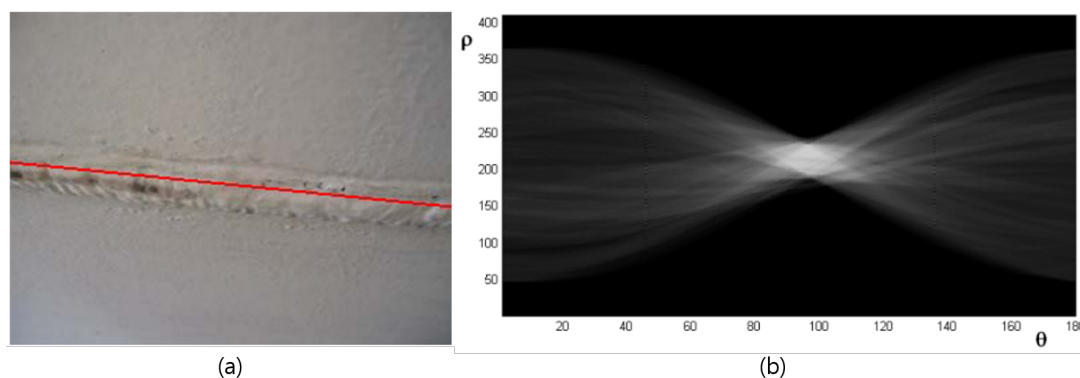


Figure 1.19: Study of detecting weld line directly using Hough transform[25]

the pre-processing.

If there is a marker in the image, the marker is regarded as a filter and detected through a convolution operation. [21], draw a marker such as figure 1.20 (b) on the target to be welded and perform template matching using the expression 1.2.

$$D(i, j) = \sum_{m=1}^M \sum_{n=1}^N |A^{i,j}(m, n) - B(m, n)| \quad (1.2)$$

In the expression 1.2, M, N is the horizontal and vertical size of the image, B is the template image found on the right of the figure 1.20 (b). $A^{i,j}$ is the image and D is the smallest value as the result of template matching. Although the above method has an advantage that it can be performed only by convolution without requiring a lot of image processing, there is a disadvantage that it is necessary to artificially create a marker in the welding plane.

All of the above-mentioned methods perform automatic welding in such a manner that the welding is detected before welding, and the welding is switched off and detected again, not in real time during welding. Therefore, there is a big disadvantage that the working speed is insignificant and it is different from the purpose of this paper to pursue fully automatic welding. The reason why it is difficult to detect the weld line during welding is due to the interference caused by the strong arc during welding. The detection method using image information is very vulnerable to the indirect due to the arc. If the exposure value of the camera is minimized in order to minimize the interference of the arc, a dark image is

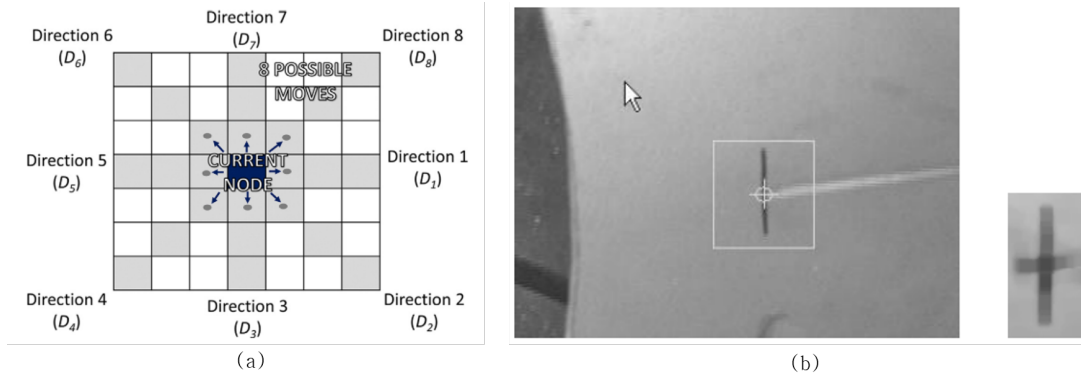


Figure 1.20: Study of detecting weld line directly using Hough transform, (a): The search range, (b): The filter used for markers and convolutions visible in the image,[21]

shown in the image so that the arc periphery cannot recognize the shape in the image. Also, the detection method using the laser is comparatively easy to detect, but the output of the laser must be very high and the size of the automatic welding device proportional increasing.

For studies that are detected during welding by arc, [23] can be mentioned. In this study, we design a filter using optics to avoid interference with the arc in the image in a passive way. In addition, an active method is also used by controlling the shutter speed and the like. However, it is used only for the flat part welding, and since the laser is not used, the computation amount of the image processing algorithm is large.

1.3 Research Objective

As discussed above, most of the weld line detection algorithms employ a semi-automatic method that temporarily turns off the welding during welding process for detection due to severe image interference of the arc occurring during welding. Therefore, the efficiency of the work is also limited and there is a disadvantage that it has to depend on the user's monitoring continuously. In addition, the algorithms for detection while welding has had a lot of drawbacks about the reliability of algorithms, and have been limited to limited types of steel such as only flat part welding.

Currently, existing equipment and studies are aimed at detecting weld seams in the absence of arcs and there is no example of complete automation to detect weld seams during welding. Therefore, in this study, a robust image that is not affected by natural light or the surrounding environment is obtained passively using an optical filter and propose a method of extracting features in images that can distinguish by using a laser on a steel which is difficult to distinguish a clear welding line because of there is no geometric characteristic. Lastly, we suggest algorithms that can be used for various types of steel with different curvatures and are highly detectable using image processing and computer vision.

The steel material to be studied will be a membrane steel sheet made by Hyundai Heavy Industries itself, and it has a flat part and a curved part at the same time. Sensor interface for image acquisition robustness against arc and detection of the welding line of steel are also accompanied.

In chapter 1, we analyze the previous research for the optical analysis of the arc and the detection of the weld line. In chapter 2, the basic idea of the optical system design and the experimental results are described. In chapter 3 explains the background knowledge about the algorithm of image processing and computer vision used in this study and explains the results of the experiment. In chapter 4 concludes and discusses future works.

Chapter 2. Design Optical System

The purpose of the optical system design described in this chapter is to acquire a certain level of image. If the two steel materials to be welded are overlapped with each other as shown in the Figure. 2.1 (a), there is a step difference, and when the laser is emitted as shown in (b), the upper and lower steel materials are distinguished in the image. In order to achieve this purpose, an arc-insensitive system is designed. In this section, we study the light characteristics of welding arc using spectroscope, and design camera, optical filter and laser for it.

2.1 Spectroscopy[31, 32]

Spectroscopy is one of the core fields of optical field, and it uses the property of light with different refractive index depending on wavelength. Past spectroscopy has been limited to analyzing spectra using the properties described above, recently, however, it is possible to estimate the information of the atomic molecular structure by detecting the amount of energy generated in the energy level jump of the electron

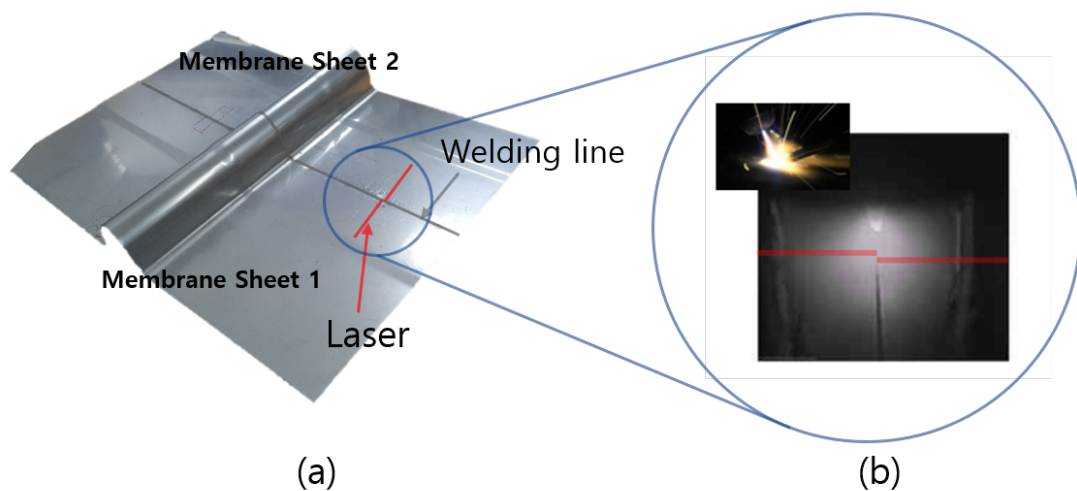


Figure 2.1: Geometric factors that cause step differences, (a): overlapped steel, (b): laser formed by steps

of a specific substance. Spectroscopes are used in many fields because they enable the characterization of materials with nondestructive testing. If the substance is not detected in a direct manner in the environmental field, absorption spectroscopy is used to determine the molecular structure. It is also used in bio-medical and space exploration.

2.2 Welding Arc Spectrum Analysis

2.2.1 Configuration of the experimental equipment

Experimental equipment such as Figure 2.2 was constructed to analyze the spectrum of the arc during welding. When the optical fiber cable is connected and the optical fiber is directed to the analyzing object, the light enters through the small hole of the fiber, and the light is scattered through the prism in the spectroscope. The scattered light is irradiated on the CCD to read the corresponding light intensity of each wavelength. The read value is connected to the computer via USB, and the PC can read the value by installing the application program provided by the spectrometer manufacturer.

The spectrometer used was HR2000 + manufactured by Ocean Optics. HR2000 + has a wavelength range of 190 - 1100 nm. It is a device that allows analysis of both near-infrared and near-ultraviolet regions, including visible light regions. This product was selected because the general absorption wavelength band of the CCD used in the camera is similar to that of HR2000+. The spectrometer uses a linear CCD and has 2048 pixels. The number of pixels is closely related to the resolution, and the product has a resolution of 1 nm. The intensity of light can be obtained by measuring the number of excited state electrons when the light is irradiated to the CCD, but only by a relative value. The maximum value is 30000, which is quantized into 14 bits and has an error of ± 1 . It has been experimentally confirmed that the minimum unit of integration time to obtain a single spectrum sample is 1 ms and the signal noise ratio (SNR) is 250: 1 to obtain a sufficiently good spectrum sample in a laboratory environment.

Experimental parameters are chosen to reflect geometric and optical properties. The position is changed to reflect the geometrical characteristics, and the reflected light and the direct light are used to reflect the optical characteristics. The spectrum analysis graph recorded on the computer is the result

of the experiment.

2.2.2 Experimental Results

As mentioned in Subsection 2.2.1, experiments were conducted with different experimental variables for various cases. As a result of the experiment, it was confirmed that the arc light was detected at the wavelength of 275-850nm. Regardless of the experimental variables discussed above, we always have the same peak point pattern, which is a reasonable experimental result based on the analysis of the reference [8] in Section 1.2.1. Therefore, if there is no new light source, the result of the spectrum is always the same in normal nature condition, and it is reasonable to design the wavelength band of the optical system based on this result.

Except for the experimental variables discussed previously, the new features of the arc identified during the experiment are the saturation case and the normal case as shown in the figure 2.3. The welding arc melts the steel through temperature control during welding and repeats the process of melting the melted steel again. Therefore, the arc does not maintain a constant brightness, but repeats the process of flashing in 4Hz, and the brightness changes continuously. Since the spectrometer generates a sample with a certain integration time, if the pixel responsible for the specific frequency component of the CCD of the spectroscope receives too much light in the integration time, it will saturate and produce the same result as in figure 2.3 (a). However, because the general case and peak pattern are constant, we do not violate the conclusion we have made.

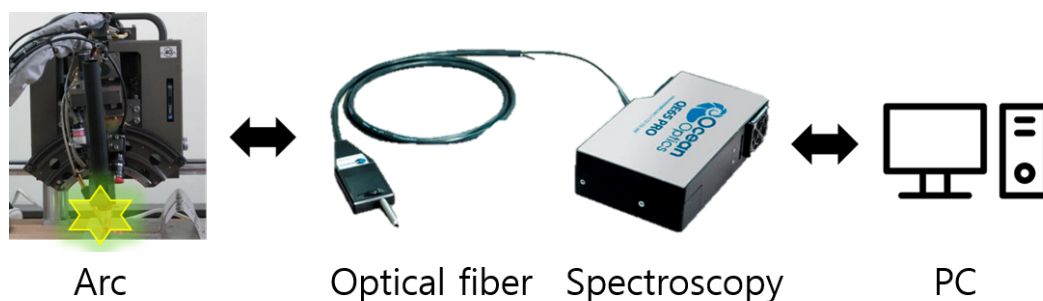
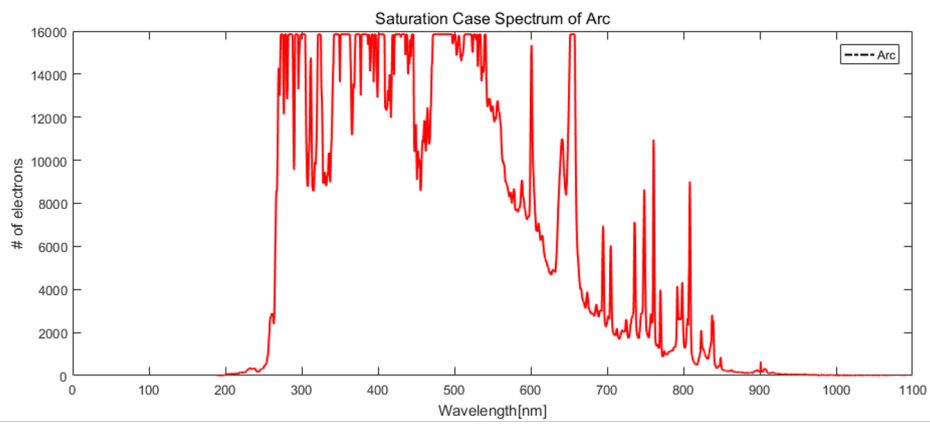
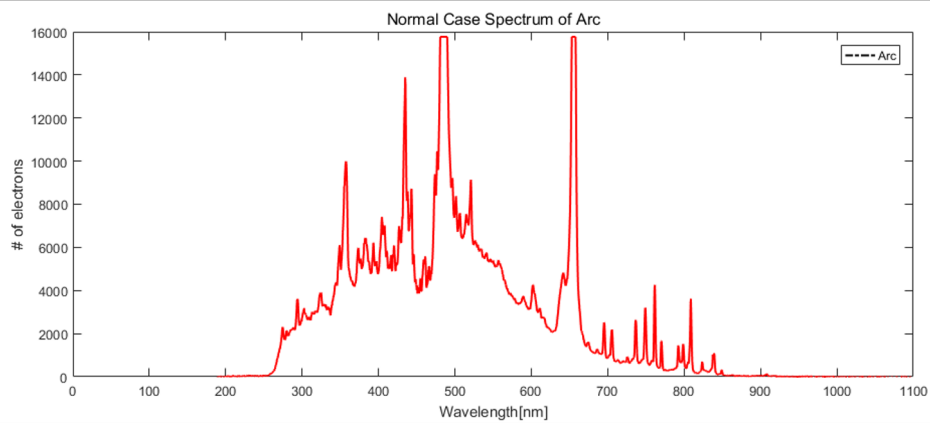


Figure 2.2: Configuration of experimental equipment for arc spectrum analysis



(a)



(b)

Figure 2.3: Results of welding arc spectrum analysis, (a) saturation case, (b): normal case.

2.3 Process of Camera Selection

Based on the results of Section 2.2, there are many spectra of the wavelength of 275-850nm and almost no detection is possible above 850 nm. Therefore, it is necessary to select an image sensor with a minimum sensitivity of 275-850nm and a sensitivity of other wavelengths. In addition, considering the environment that can be tested in the present Mark III, it should have a minimum dimension of 30mm*30mm*30mm

In order to reduce the noise in the image for detecting the weld line, it is necessary to secure a large number of frames to increase the detection number. Considering the welding speed (300mm/min), welding is performed at 5mm per second 4Hz, and the shiny welding torch hinders the image quality when the maximum brightness is achieved, it is necessary to secure 5 or 6 frames per unit length(mm). Therefore, camera with a minimum frame rate of 30 frames per second must be selected. You will also need to a camera model that provides software development kits(SDK) to control camera parameters such as camera exposure.

In addition, the image sensor must select between CCD and CMOS sensors. In the case of a CCD, a signal is received by each pixel and amplified by an amplification amplifier through a transfer resistor. However, when reading the value while transferring the amount of charge accumulated in the charge well to the row or column, if a charge overflows to a specific pixel, the peripheral portion and the row and column to which the pixel belongs are influenced and a bloom-smear phenomenon occurs as in the figure 2.3. In the figure 2.3, the orange circle is clearly visible around the headlight of the locomotive, and the purple line passing through the headlight is a smear phenomenon[33]. Therefore, it is advantageous to use a CMOS sensor when the brightness of the image is bright like the welding torch and the charge saturation phenomenon is frequent in the sensor.

2.3.1 Determining Camera Absorption Wavelength

Considering the wavelength band of the desired region, the NIR(Near-Infra-Region) Camera has a choice but the camera which absorbs the wavelength of 850nm or more without absorbing the wavelength

of the visible ray region is usually classified into the infrared camera group and it is a very expensive camera. Also, if you look at the manufacturer's data sheet 2.5, you can see that the average center of the absorbed wavelength has shifted to the near-infrared region, rather than completely receiving the visible light region. Therefore, it is more reasonable to select a camera that absorbs more than 850nm wavelength in general machine vision cameras and overcome the other wavelengths with additional optical filters.

2.3.2 Determining Camera Model

The summary of the discussion at the beginning of Section 2.3 is as follows. (1) absorbs wavelengths of 850 nm or more, (2) constraints on the standard, (3) 30 frames, (4) possibility to control camera parameters, (5) using CMOS sensor. The USB 3.0 Flea3 camera group provided by Point Gray satisfies (2), (3), and (4). In addition, the software provided by the inside allows easy control of camera parameters and SDK, which makes it easy to manufacture sensor boards later. The camera, FL3-U3-20E4C-C, is the camera that shows the highest rate of absorption in the 900-nm wavelength band, with most cameras satisfying (1) but satisfying (5).



Figure 2.4: bloom-smear phenomenon [33]

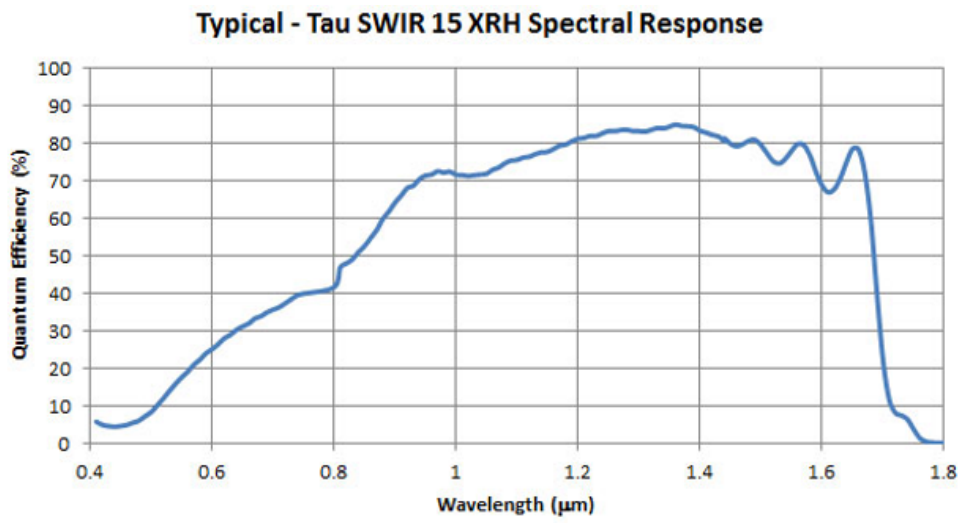


Figure 2.5: Spectral response graph of infrared camera[34]

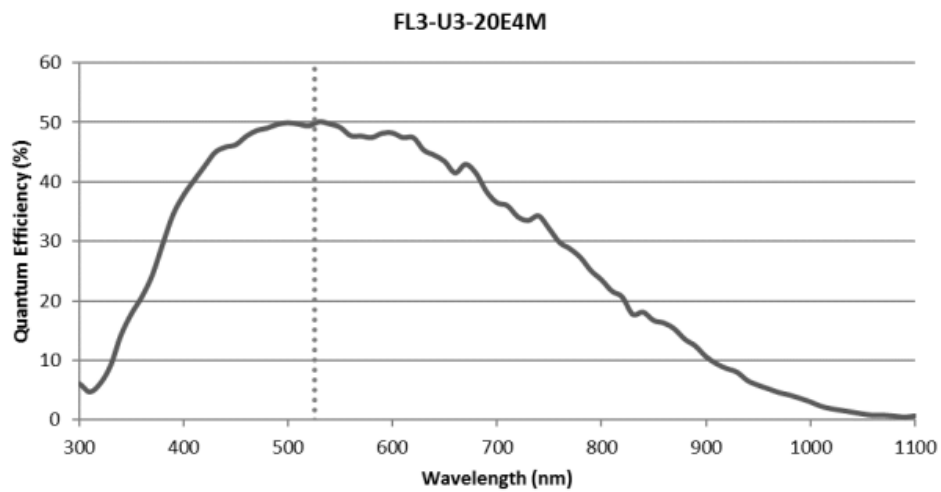
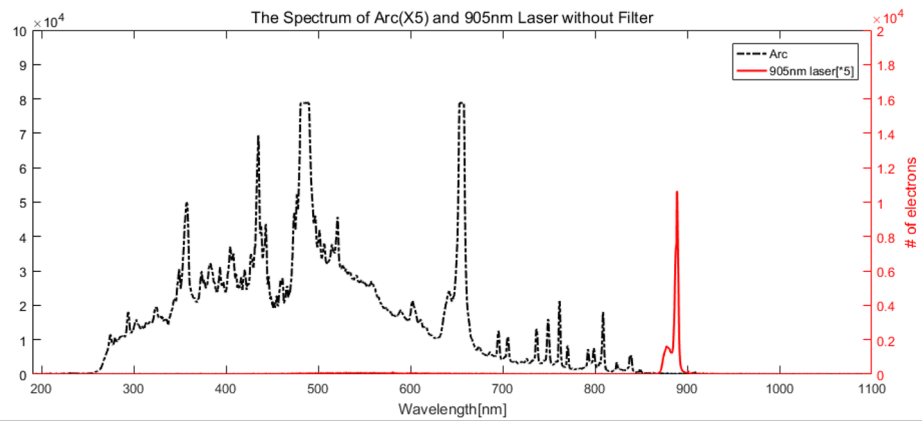


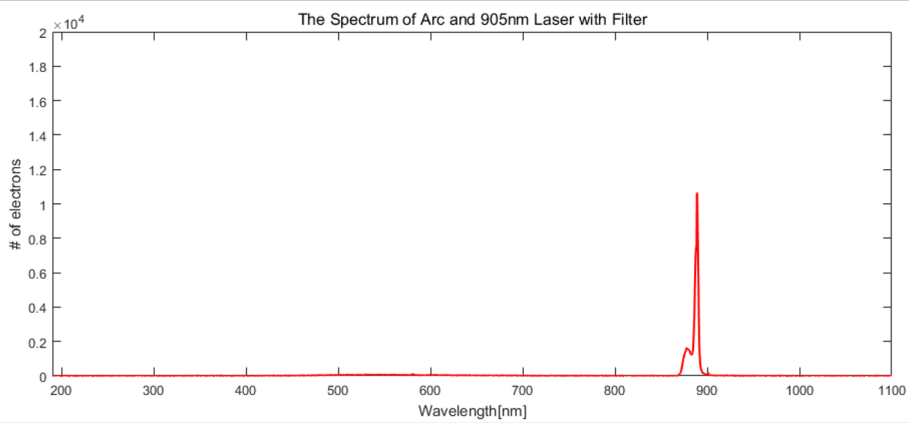
Figure 2.6: FL3-U3-20E4C-C Camera's Spectral response[34]



Figure 2.7: FL3-U3-20E4C-C camera model of Point gray[34]



(a)



(b)

Figure 2.8: Estimated spectral response graph: (a) Spectral estimate of arc and laser, (b): Estimated result of improved spectrum with filter

2.4 Process of Optical Filter and Laser Selection

An optical filter attaches a special film to the lens to pass only the desired wavelength band. Filters are one of the most basic materials in the field of optics, so many companies deal with a wide range of wavelengths to choose. Considering that the laser also has a wavelength band of 850 nm or more, it is conceivable that the spectrum in which the arc and the laser are mixed is the same as (a) in the figure 2.8, as shown in (b), it is necessary to effectively control the spectral region constituting the main component of the arc by the filter so that only the laser spectrum component remains.

2.4.1 Principles and Terminology of Optical Filter[25]

This section roughly examines the characteristics of these filter types and summarizes the terms necessary for filter selection.

Optical filters can be broadly divided into absorptive and dichroic. The absorptive filter absorbs light according to the absorption characteristics of the filter used. It make the absorptive filter suitable when the noise generated by the unwanted light wavelength is fatal to the system, and it is insensitive to the angle because it can absorb light of various angles. However, the disadvantage is that the durability is easily worn out.

Separately, the dichroic filter reflects unwanted wavelengths and transmits the desired portion of the spectrum. The light passing through a medium with a low refractive material by stacking materials with various refractive indices such as a figure 2.8 is obtained by utilizing the interference characteristics of light reflected from a medium with a high refractive material. The dichroic filter based on reflection by Snell's law is very sensitive to angles. When using light other than the design angle, the design result is out of order.

The Figure 2.10 summarizes the picture to explain the key optical filter terms. The central wavelength indicated in (a) is defined as the center point between wavelengths where the percent transmission is 50% of peak transmittance and is called FWHM (full width at half maximum). Since the manufactured filters follow a Gaussian distribution, they are also commonly used with a maximum transmittance of

a bandpass filter or a maximum reflectance of a notch filter. Bandwidth is the wavelength range that represents a specific region of the spectrum that passes the energy incident through the filter.

(b) describes the blocking range. A blocking range is a term used mainly in a band blocking filter. The blocking range is defined based on a band corresponding to 50% based on the lowest point like a bandwidth. The term optical density (OD) is used when expressing the blocking range in a filter other than a blocking band filter. it is mathematically defined by the formula 2.1.

$$OD = -\log\left(\frac{T}{100}\right) \quad (2.1)$$

T means the transmittance(%). As mentioned , the higher the OD , the lower the transmittance. A dichroic filter is a type of filter used to transmit or reflect light as shown in Figure (d). Certain regions are reflected or absorbed and are mainly used for long bandpass filters or short bandpass filters. (e) and (f) illustrate the cut-on wavelength and the cut-off wavelength. The cut-on wavelength means the wavelength at which the transmittance increases to 50% throughput, and the cutoff wavelength accounts for the wavelength at which the transmittance decreases to 50% throughput.

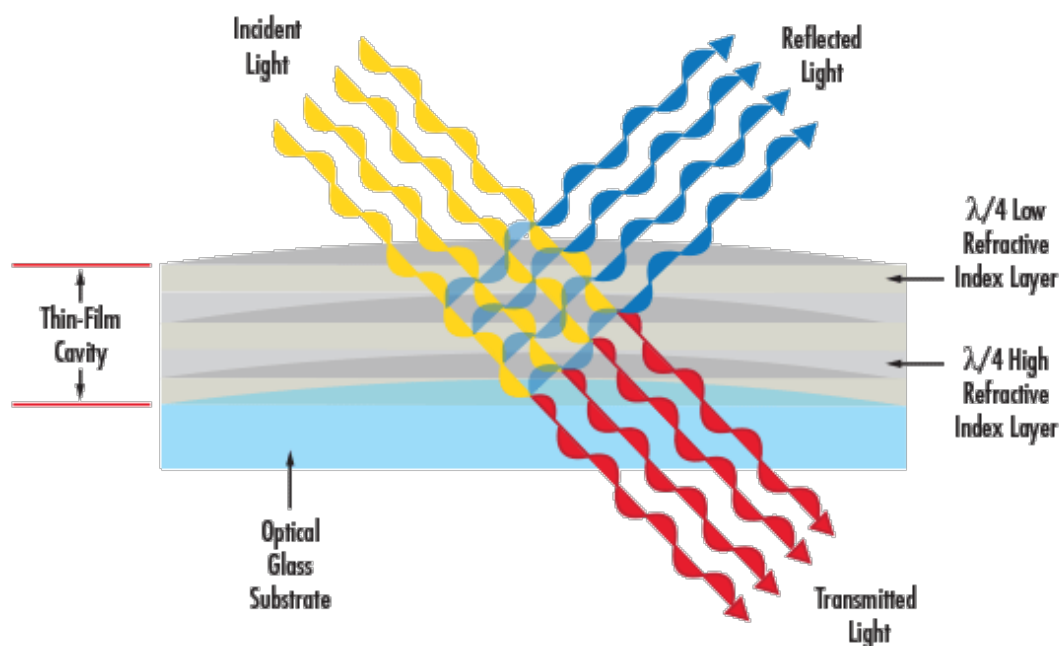


Figure 2.9: Principle of optical filter[35]

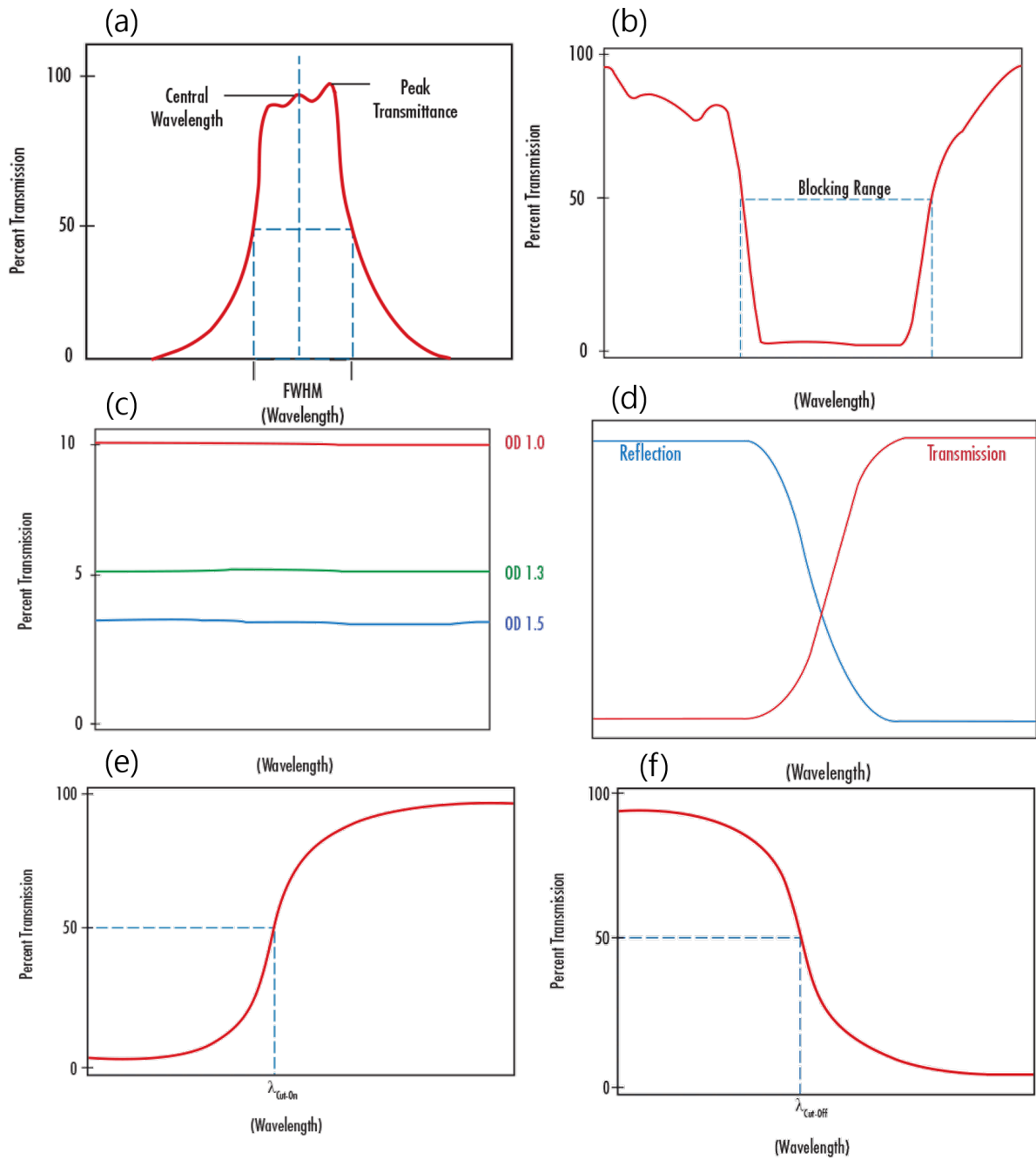
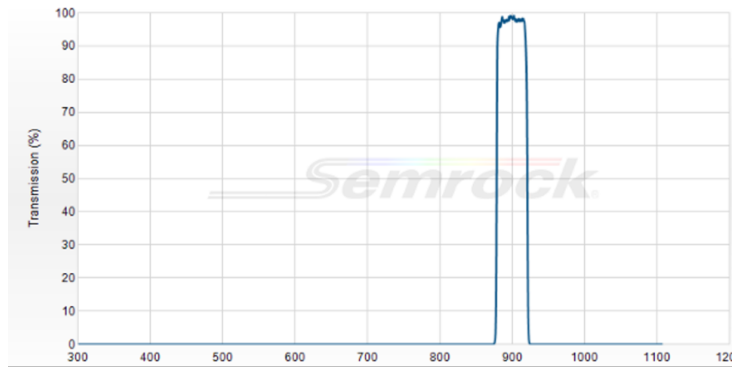
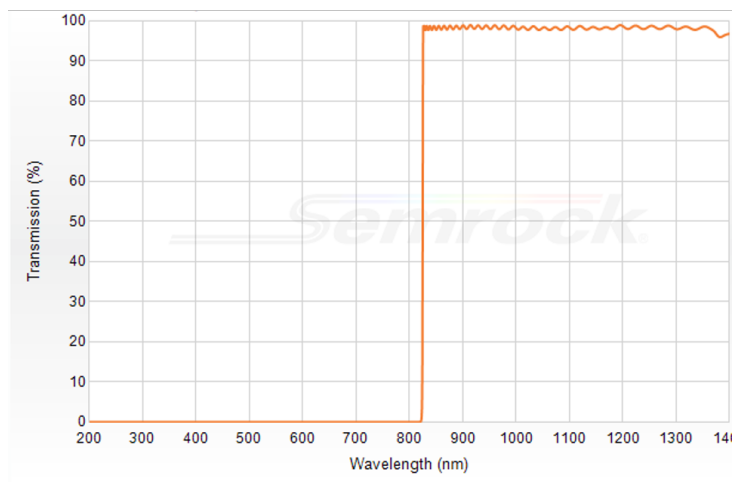


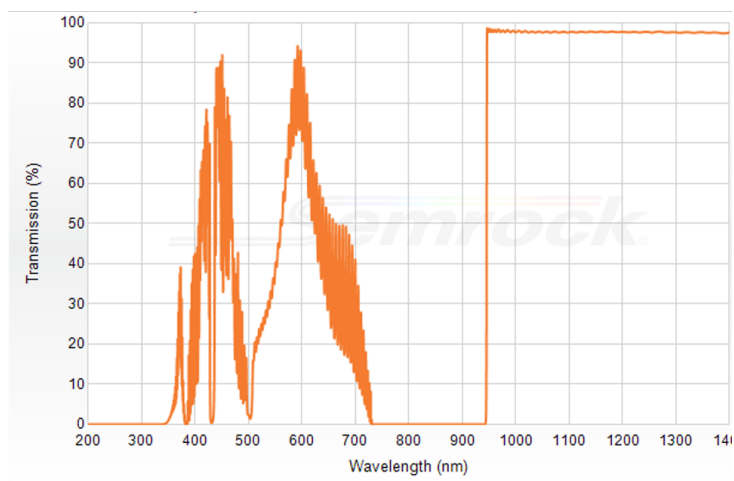
Figure 2.10: The graph for illustrate optical filters Terminology[35]



(a)



(b)



(c)

Figure 2.11: Filter spectrum response graph, (a): 905nm system filter, (b) 980nm system filter 1, (c) 980nm system filter 2[36]

2.4.2 Constraints and Selection of Optical Filter

As mentioned in Section 2.3 and 2.4, the filter must pass wavelengths above 900nm, blocking the wavelength of 275-850nm. In addition, the light entering the blocking band camera (arc) is very strong so must meet OD 5.0, the highest level of blocking of the optical filter. It will mention in the following subsections, however, we have two wavelengths, 905nm and 980nm. Plus, both systems were tested by selecting a filter that can show the laser at the maximum angle of view of 30 degrees

The filter in the 905nm laser system were chosen to have filters with FWHM;30nm to reflect the characteristics of the varying filter. Filters manufactured by American filter maker Semrock have a blocking band of 200-866nm, 935-1100nm, a passband of 884-917nm, and a center wavelength of 900nm, as shown in figure 2.11 (a). The FWHM meets all the constraints mentioned above at 43nm.

The filters in the 980nm laser system cannot select the desired filter band, so two filters were used. We implemented a filter that cuts off 950nm by combining two filters, a filter of Figure 2.11(b) and a long-pass filter of filter (c). Blocking band is 200-950nm, passband is 950nm - 1100nm. The blocking-band is 200-950nm and the passband is 950nm-1100nm. The cut-off frequency is 950nm.

2.4.3 Constraints and Selection of Laser

The diode of a laser uses light emitted when a single wavelength laser theoretically emits electrons. Therefore, it is not possible to make lasers of all the wavelength bands, but the choice is relatively limited. Above the 850nm wavelengths, It is possible to choose 860, 880, 905, 945, 980nm, and it is recommended to have an at least 50nm buffer band from which an arc exists. Therefore, a laser diode with a wavelength band of 900 nm or more must be selected.

As can be seen from the image sensor information of Figure 2.7, the sensitivity of the image sensor in the near-infrared region decreases in proportion to the wavelength, so if the wavelength is over 1000nm, the image with high noise is obtained. Therefore, it was judged that the wavelength bands of 905 nm and 980 nm were most reasonable.

Also, as can be seen in previous literature review for seam detection, it is necessary to output a

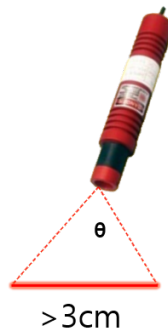


Figure 2.12: Laser irradiation angle

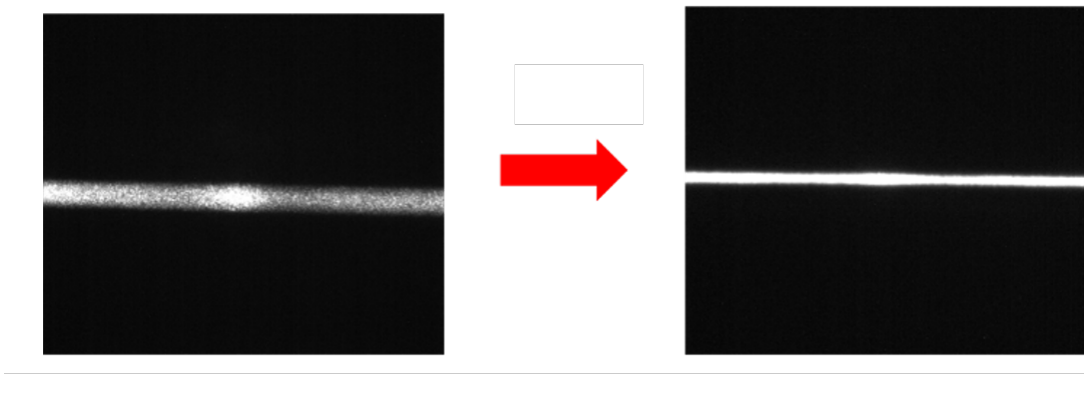


Figure 2.13: Results obtained by reducing laser width

laser to artificially characterize through the image. Because it is difficult to distinguish between normal point shape type lasers, a linear laser is used by attaching a diffraction lens to the laser head.

In the beginning of Section 2.3, as mentioned in the selection of the camera, the size of the welding robot is fixed and there is not much free space. Therefore, in the experimental stage, a laser with a length of 80 mm and a diameter of 20 mm or less should be selected.

In the case of the output power, it is difficult to know the absolute intensity of the wavelength band of 900nm or more of the arc that can be obtained by the spectrum analysis, so it is decided by the method using proportional calculation. Generally, the output of the laser used in the literature is within 10mW. It can be considered as an output power that can be detected without difficulty in the image since it does not proceed simultaneously with welding. The spectral results of the current 905nm 100mW laser and the measured spectra of the arc showed about 3-4 times difference in the relative intensity of 905nm.

The detection position is within 1cm from the welding arc required by the actual industry. Considering that the intensity of light decreases with distance from the light source, it is necessary to output more than 50mW to see the laser at 1cm. However, the 300 mW high power laser is beyond the size limit because it requires additional cooling and driver parts with a high-performance controller. In this study, we aimed at the simultaneous operation with the welding robot, so we considered the minimum power of 50mW. Plus, a laser with adjustable power of 150mW with a minimum output power of 50mW was selected.

The laser length control through the diffractive lens is represented by the angle of the laser beam as shown in figure 2.12. Considering that the amplitude of the disturbance required in the industrial field is 3cm, laser strip length should be higher than 3cm. The fixed height length between the welding torch and the laser diode is 10.5cm, so θ should be 15° ,

In order to maximize the intensity of the laser light in the image, it is necessary to reduce the laser irradiation area. The point where the diffraction width is the minimum is experimentally found. As a result, the width of the laser was reduced to the maximum as shown in the figure 2.13.

2.5 Experiments and Results

2.5.1 Experiment Configuration

The side and back side of the design drawing of the figure shown in figure 1.3 is shown in figure 2.14. The laser and camera were attached as shown in figure 2.15. The Figure 2.14 (a) and (b) are the torch parts of the welding robot, (c) and (d) are the parts that fix the torch part, and the design can be changed if the torch can be fixed. (e) and (f) show the designable range. When welding, rotate the torch up to 69.6 degrees. Therefore, it should be located within the red range shown in (e). Otherwise, it is very dangerous to generate mechanical interference during welding. (f) is a description of a space that can be designed in the welding robot. The part that fixes the welding torch and the part of the welding torch can move because it has a degree of freedom about the horizontal axis based on the side view.

Considering these movements, the part shown in (f) is actually a part where no mechanical inter-

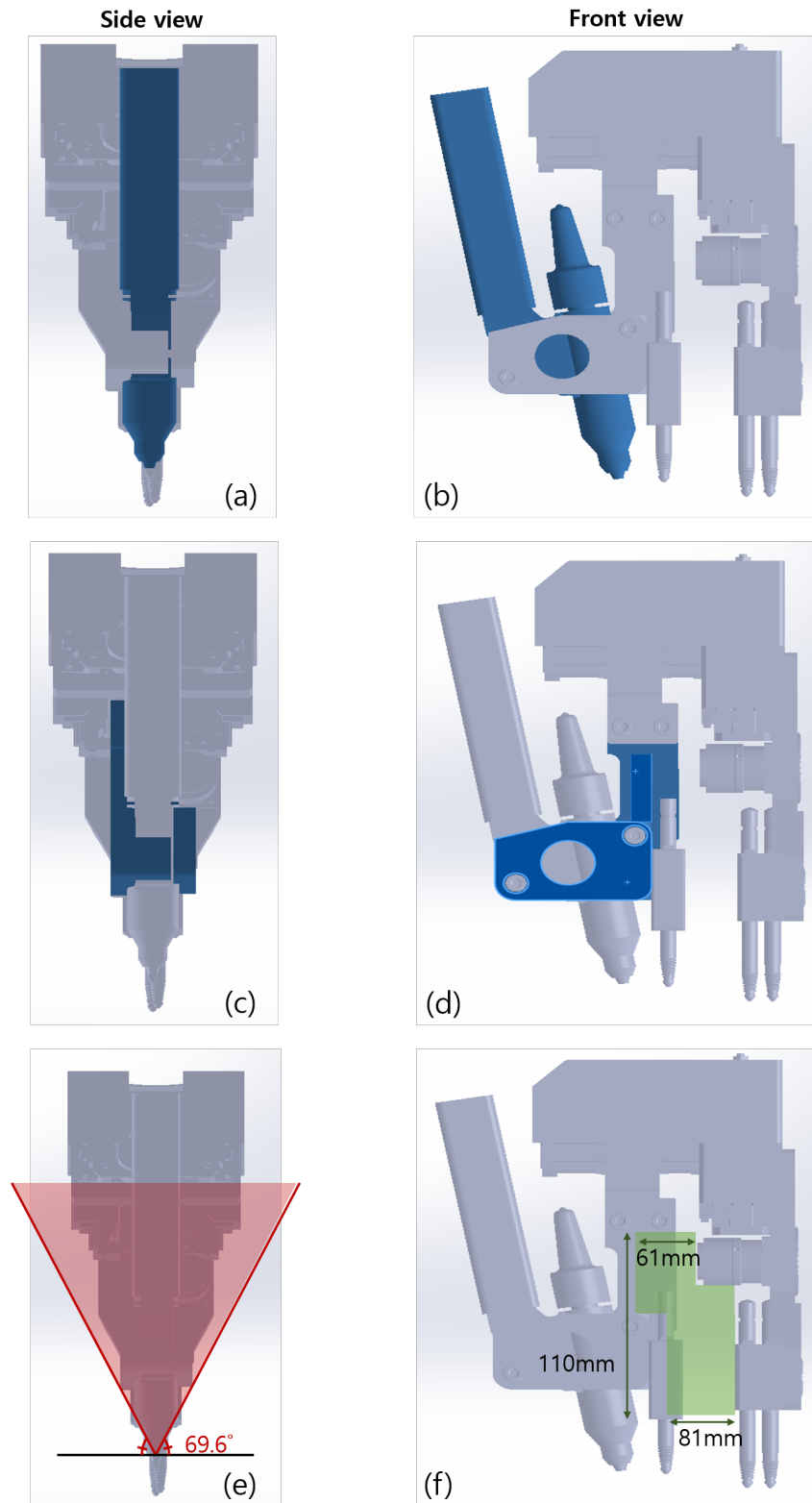


Figure 2.14: Welding robot step file, (a), (b): Welding robot torch part, (c), (d): Welding robot torch fixing part, (e), (f): Range of welding robot design

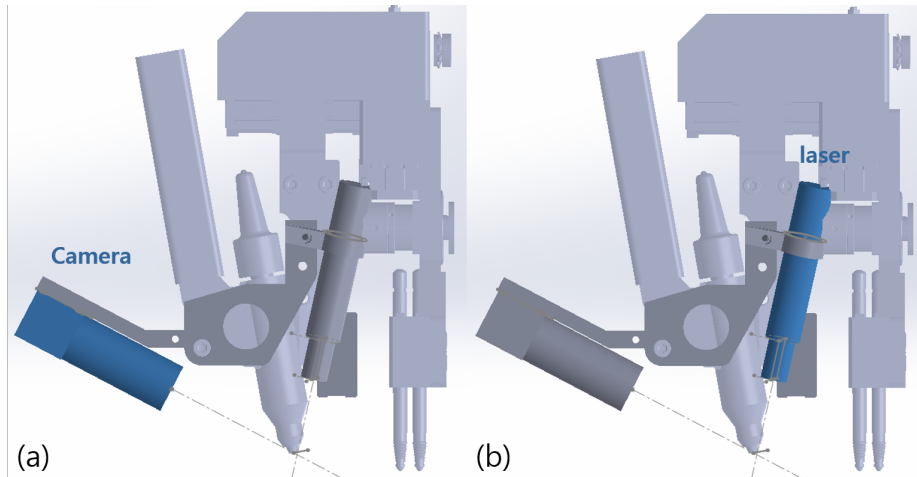


Figure 2.15: Welding robot shape after attaching optical system, (a): camera, (b): laser

ference occurs during welding. The figure 2.15 is the image after the optical system is designed. (a) is a camera, and (b) is a laser. Experiments have shown that no mechanical interference occurs during welding.

2.5.2 Results

The Figure 2.16 is a photograph of the experimental results before and after the optical system design. (a) and (b) were photographed at a shutter speed of 4 ms, and shutter speed was a decisive factor in controlling the exposure amount of the camera. Additionally, The exposure amount is determined by the shutter speed, the image sensor gain value, and the aperture value. Among them, the aperture reacts most sensitively and gain and shutter speed respectively. Because the arc is so strong that it can not be seen with the naked eye, it experimented with adjusting the aperture and gain to the minimum and the most insensitive shutter speed. The shutter speed is a minimum of 0.1 ms to a maximum of 25 ms. When the shutter speed is high, the image becomes brighter. When the shutter speed is lower, the image becomes darker. If the shutter speed is increased, the interference of the arc becomes stronger as the image becomes brighter, making detection difficult. Also, if the shutter speed is lowered, the brightness of the laser part becomes dark, so that the noise of the sensor becomes worse and the detection becomes impossible.

The figure 2.16 is the image taken with a shutter speed of 0.1m, 4ms. (a) and (b) show the maximum

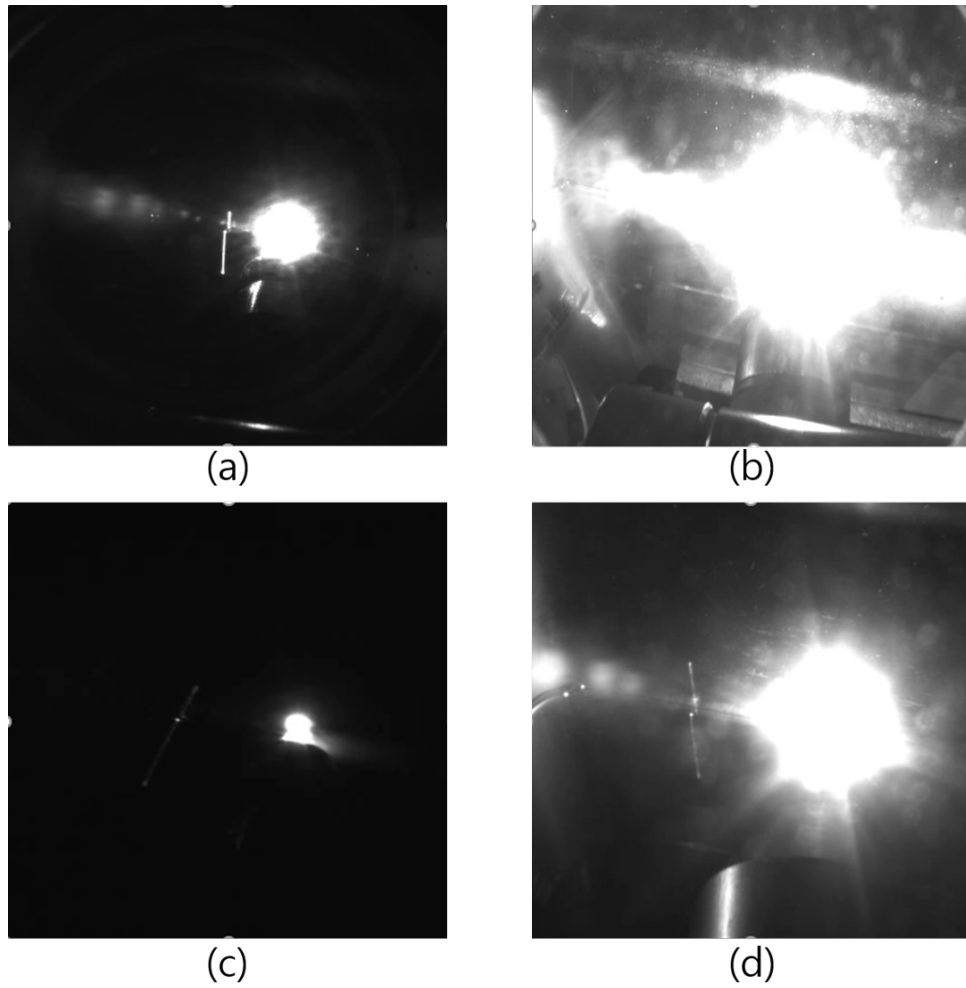


Figure 2.16: Comparing the results before and after attaching the optical system, (a): After attaching the optical system(Shutter speed 4ms), (b): Before attaching the optical system(Shutter speed 4ms), (c): After attaching the optical system(Shutter speed 0.1ms) (d): Before attaching the optical system(Shutter speed 0.1ms)

arc interference at the detectable range (4 ms). (c) and (d) illustrate the effect of reducing the shutter speed to a minimum and show the effect of the optical filter visually. (a) can be confirmed that the laser can be sufficiently separated from the laser part although there is some interference of the arc. (B), on the other hand, the laser part is completely hidden from the interference of the arc. (c) can confirm the degree to which the interference of the arc is removed by the filter. (d), Even though the arc interference is minimized by adjusting the shutter speed, it can be seen that the interference of the arc is very strong compared to (a) which receives 40 times higher light amount.

The 905nm system and the 980nm system is shown in figure 2.17. The laser output condition and

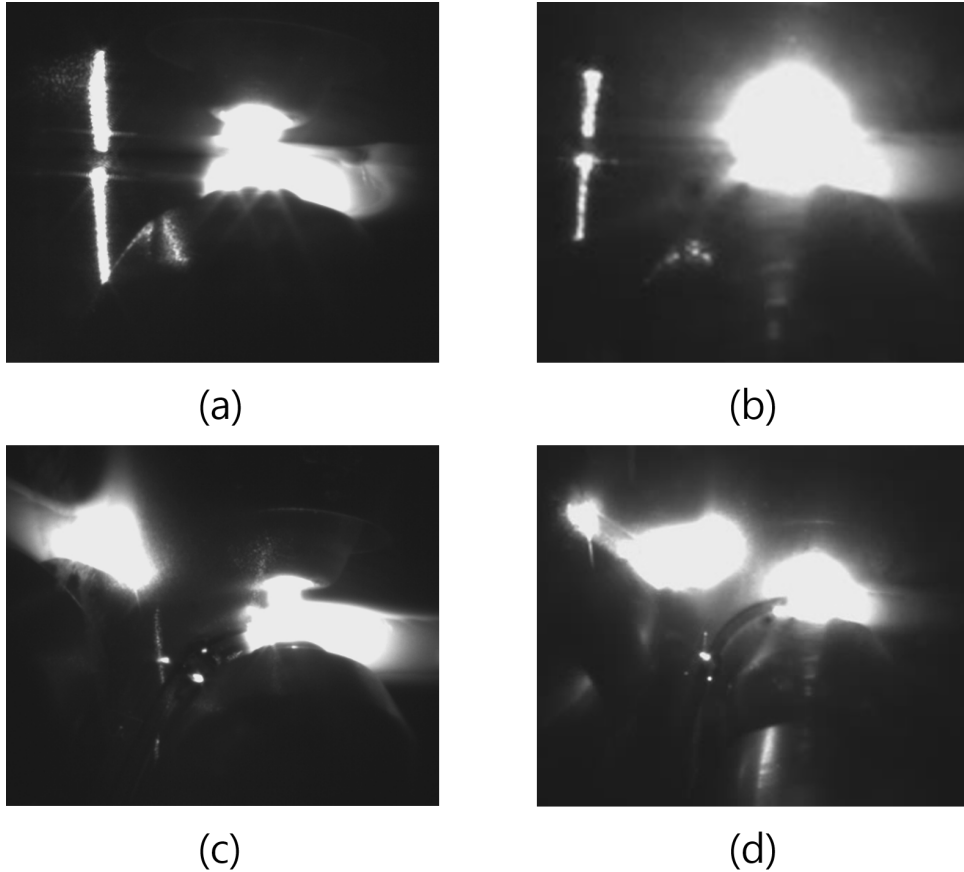


Figure 2.17: Comparison of 905nm and 980nm laser system, (a): Flat Region of 980nm System, (b): Flat Region of 905nm System, (c): Flat Region of 980nm System, (d): Curved Region of 905nm System.

angle were under the same conditions. (a) is a flat region image of the 980nm system and (b) is a flat region of the 905 system. (c) is the image at the entrance of the curved surface of the 980nm system. The right bright circle is the torch and the left is the part where the torch is reflected on the curved part. (d) is the image at the entrance of the curved surface of the 905 nm system. It confirm that the 980 system shows better performance so that it can be distinguished from the images of 905 system and 980 system. It implies even a few of the arc, it is also present above 900 nm and the amount of light is proportionally decrease as the wavelength gets longer.

Despite designing the optical filter, there are two reasons why the light can be seen in the picture. The first is the assumption that light will also come in the pass-band of the filter. It can be demonstrated as a result of the 905 nm system and the 980 nm system. Both systems used filter combinations with similar ODs in the 200-850 nm band. Since the remarkable difference between the two systems is only

the wavelength band of the pass-band, the difference in the amount of light seen in the cameras of both systems shown that the amount of light coming from the pass-band is different.

The second factor can be considered to be some light in the cutoff band. 2.1 is formula of filter OD. In the experiments, The filter OD is 5. Therefore, the light of the cutoff band comes in at a rate of 0.1%. Since the light intensity of the arc is very high, the photons in the ratio of 0.1% cannot be ignored and the arc is visible in the image.

A small arc is shown in the image, but there is no difficulty in detecting it using the algorithm to be introduced in the next section. Relatively, the advantage to be obtained at an additional cost is lower. As a result, the optical system of 980nm is used.

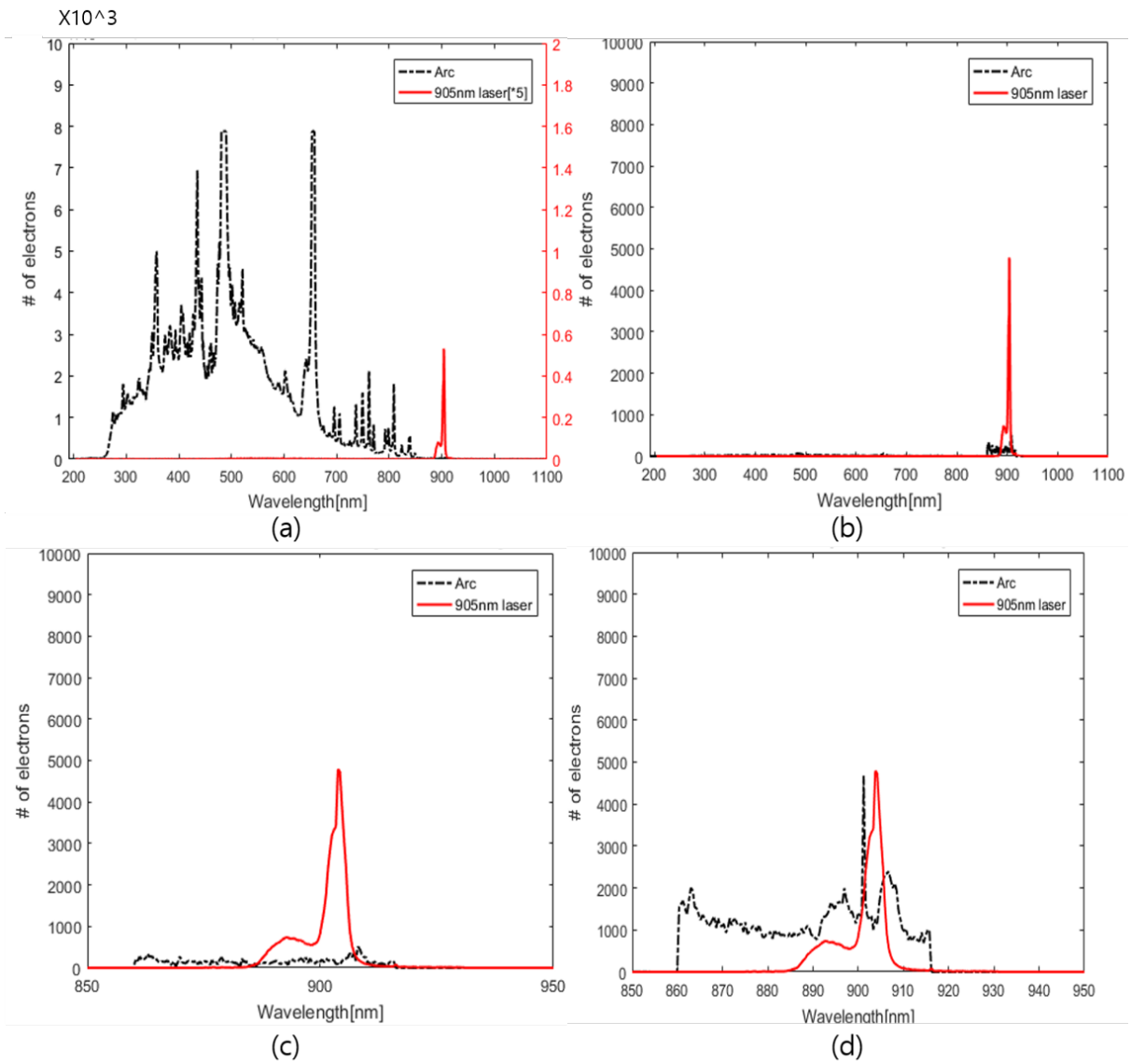


Figure 2.18: Result of 905nm optical system, (a): Non-filter case, (b): Filter Case in unsaturation, (c): Filter Case in unsaturation(850-950nm), (d): Filter Case in saturation(850-950nm).

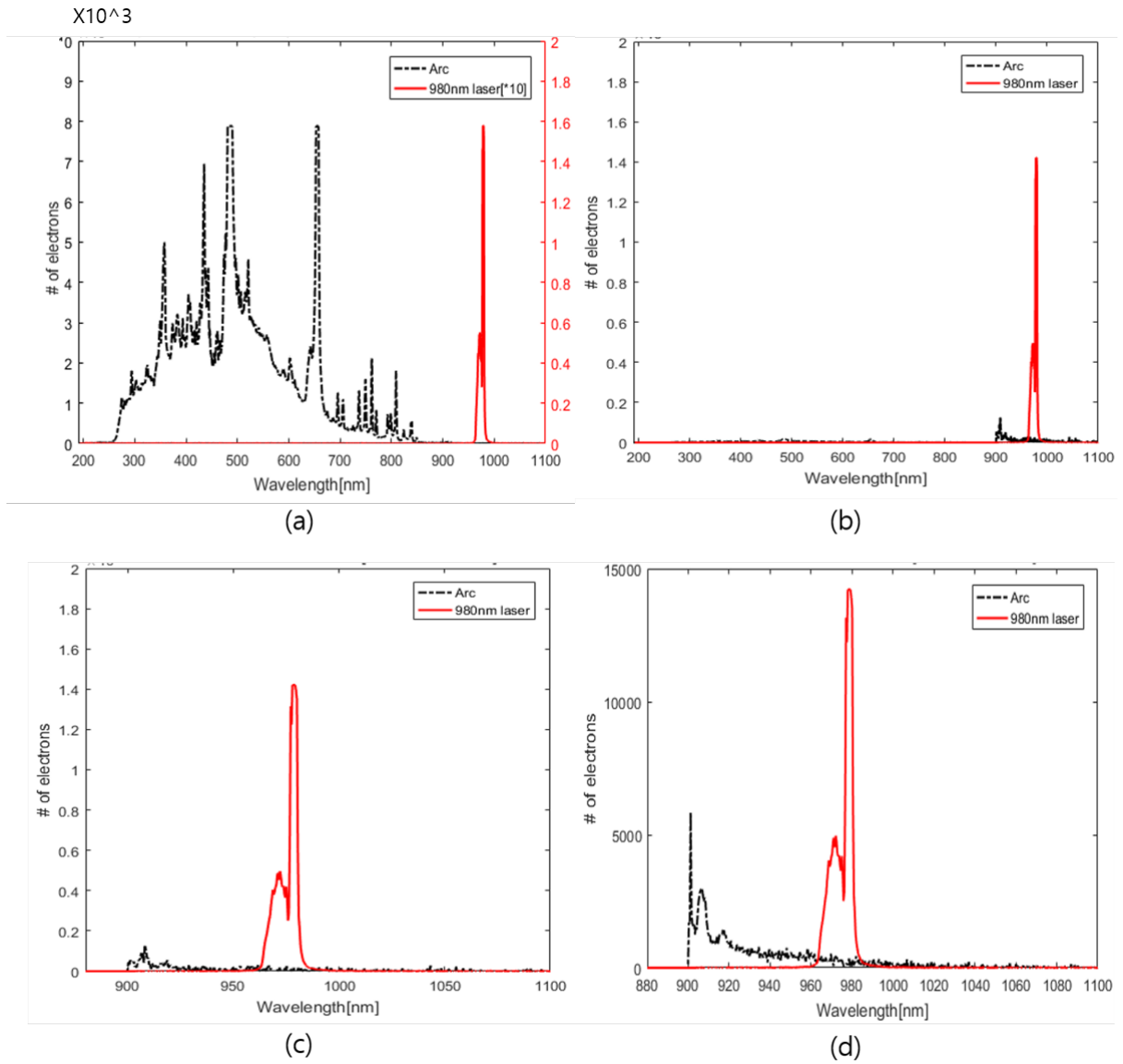


Figure 2.19: Result of 905nm optical system, (a): Non-filter case, (b): Filter Case in unsaturation, (c): Filter Case in unsaturation(880-1100nm), (d): Filter Case in saturation(880-1100nm).

Table 2.1: Power Ratio Result of Optical Systems; Maximum exposure and minimum exposure mean the case of the saturation and unsaturation in spectrometer, respectively. Power ratio calurated by power ratio = $\frac{\sum_f |X_L(f)|^2}{\sum_f |X_A(f)|^2}$. $X_L(f)$, $X_A(f)$ mean the spectrum of laser and arc, respectively

	Maximum exposure		Minimum exposure		
	value	%	value	%	
Power ratio	980nm filter	0.89	89%	6.5	650%
	905nm filter	0.24	24%	1.53	153%
	without filter	0.0009	0.09%	0.0043	0.43%

The overall results are summarized in the following graphs the figure 2.18, the figure 2.19 and the tables 2.5.2.

The figure 2.18 is (a) of the 905nm system is the spectral result of the arc and laser when filter isn't used. In unsaturation case, note that the size of the y-axis, which is the size of the arc and laser, is five times the difference. (b) is a graph using a filter when it is not saturated. (c) is a spectrum in which (b) is further enlarged and only the main components are observed. (d) is a spectrum when saturated. As implied in the graph (d), if it is saturated, the components of the arc are still too much to be detected.

The figure 2.19 is (a) of the 980nm system is the spectral result of the arc and laser when filter isn't used. In unsaturation case, note that the size of the y-axis, which is the size of the arc and laser, is five times the difference. The spectral results also increased due to the increase in laser power. (b) is a graph using a filter when it is not saturated. (c) is a spectrum in which (b) is further enlarged and only the main components are observed. (d) is a spectrum when saturated. It is observed that arc components is very few differently from the figure 2.18-(d)

The results are quantitatively summarized in the table If the filter is not present, it is very small, about 0.43%, based on saturation. It increased to 24 % at 905nm and to 89 % at 980nm system. Significantly increased spectral results lead to good quality images, which do not require complex image processing. This is discussed in detail in the chapter 3.

2.5.3 Conclusion

In Chapter 2, the design of the optical system and results of the experiments attached to the welding robots are presented. As seen in Chapter 1, there are very few cases where an optical filter-based optical system is applied to actual welding robots. This is because arc is the worst condition for applying computer vision in automation perspective, and hence many studies presume the absence of arc. Therefore, the lack of a wide range of considerations has led to the limitations of fully automated welding. As we can see from the experimental results of the optical system in this chapter, we succeed in reducing the influence of the arc, which is the primary purpose of the study. We succeed in obtaining a high-quality image, which enables us to detect the weld line not only the flat surface but also the curved surface. It allows real-time weld line detection, otherwise remaining as an unsolved problem.

Due to cost limitations, currently used mass-produced filters have not been able to adjust a spectral response arbitrarily. In addition, there exist several problems regarding camera viewpoint when entering the curved surface and mechanism interference due to look-ahead distance. However, there is a potential improvement when considering the fact that the optimum filter overcomes the cost limitation by the application of mass production, in which the mechanism interference by the robot design change can be minimized. Therefore, it can be possible to make a fully automatic welding robot by employing the optical system proposed in this study.

Chapter 3. Welding Line Detection

This chapter covers the detection of weld lines based on the images obtained in Section 2. It consists of background knowledge, research contents and conclusions to understand the research largely. Section 1 explains basic background knowledge, Section 2 introduces basic knowledge of computer vision, Section 3 explains the whole process, and then explains applied image processing and computer vision algorithms. In the final Section, we conclude with the experimental results and discussion.

3.1 Background of Image Processing

Image processing is roughly classified into three types. The first is the image processing technique using the histogram of the image [38]-[46]. It is mainly used to control the saturation, brightness, etc. in the image by [45]-[43]. It is also a method used mainly when there is a clear target color such as extraction and elimination of a specific color by directly controlling the color space. For example, real life such as removing fog and overcoming illumination differences by illumination is also used [46]. In recent, there is also a case where a histogram is used to extract feature points from images [38]-[40].

The second is to use a spatial filter in image space [47]-[52]. The method using a spatial filter is implemented through convolution-based cross-correlation. The spatial filter mainly uses image enhancement for the purpose of removing noise, and may be used as a preliminary step to obtain information in the image, such as [49]-[51] edge information[47, 48, 52]. This paper mainly explains the latter.

The third is to use a spatial filter in the frequency domain[53]-[56]. Because the image is the result of the analysis of the electrical signal, it is possible to convert it to the frequency domain using a two-dimensional Fourier transform. Therefore, there is also the theory of specific frequency elimination through frequency filter design in the frequency domain. However, this study does not use image processing to deal with frequency bands, so it is not mentioned in the paper.

3.1.1 Image Enhancement using Histogram Transformation

The histogram is a graph of the frequency distribution in the language used in statistics. More simply, the frequency distribution table is a graphical representation. Normally in histograms, a x-axis and y-axis mean class and frequency respectively[57]. In the image, the pixel value means the class, which means the x-axis, and the number of pixels means the y-axis [58].

For example, when a histogram of a gray image is drawn, it can be expressed as 3.1. Here, the x-axis is the size of the pixel of the image expressed by 8 bits, and ranges from the darkest 0 to the brightest 255. The y-axis represents the number of pixels having the same pixel value.

By using the histogram, you can roughly estimate the contrast without looking at the image. As you can see in the Figure 3.2, the left camera picture has the most black, the darkest among the three pictures, the middle one has the middle brightness, and the right picture is the brightest picture. Therefore, the histogram of the left figure shows that there are many dark pixels and it is shifted to the left much, and

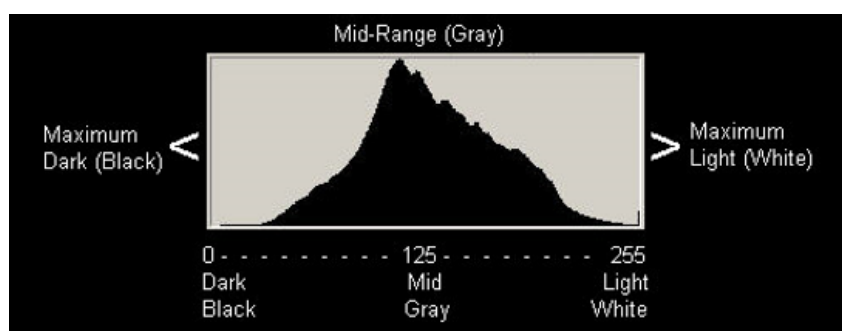


Figure 3.1: Image histogram

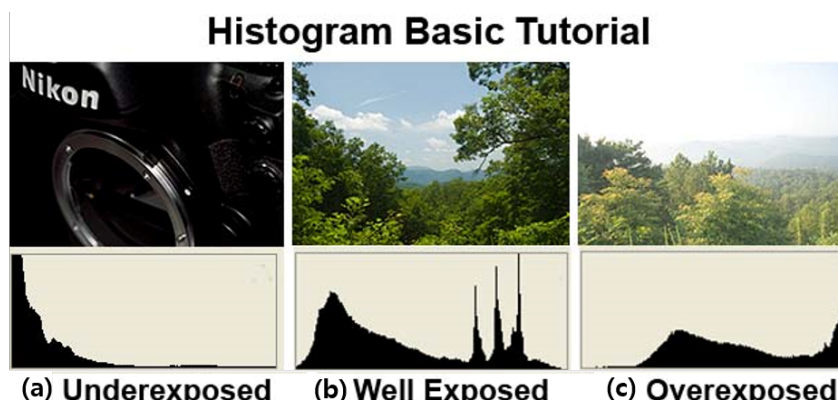


Figure 3.2: Histogram results of images with different brightness, (a): low brightness image, (b): medium brightness image, (c): high brightness image.

the center figure spreads evenly in the middle, and the right figure is much shifted to the right. In this way a histogram is a good means of representing information in an image.

3.3 (a) and (b) clearly distinguish between relatively bright and dark photographs. (a) is darker and (b) is brighter. Imagine the case in which a person who recognizes that a photograph like (b) is "better" gets a photograph (a). Definitely want to make a picture like (b). It is a histogram transformation that makes this possible, and it is used in the real world too[45] - [43].

Histogram transformation allows you to change the histogram of an image to the shape you want. A typical transformation function is a method using gamma function and is called gamma correction. gamma function is defined as follows.

$$y = x^{\frac{1}{\gamma}} \quad (3.1)$$

Here, x represents the pixel value of the image pixel before correction and y represents the pixel value of the pixel corrected by gamma transformation and γ is the correction parameter which is higher than 0. For example, in 3.4, when the pixel value of the input image is 128, it has a higher pixel value by a gamma transformation greater than 1, and a lower pixel by gamma transformation between 0 and 1. Therefore, if it is larger than 1, the image becomes brighter. If it is between 0 and 1, the image becomes darker. This can also be seen in the result of 3.5.



Figure 3.3: Two images with different brightness of the same subject, (a): a relatively dark image, and (b): a relatively bright image.

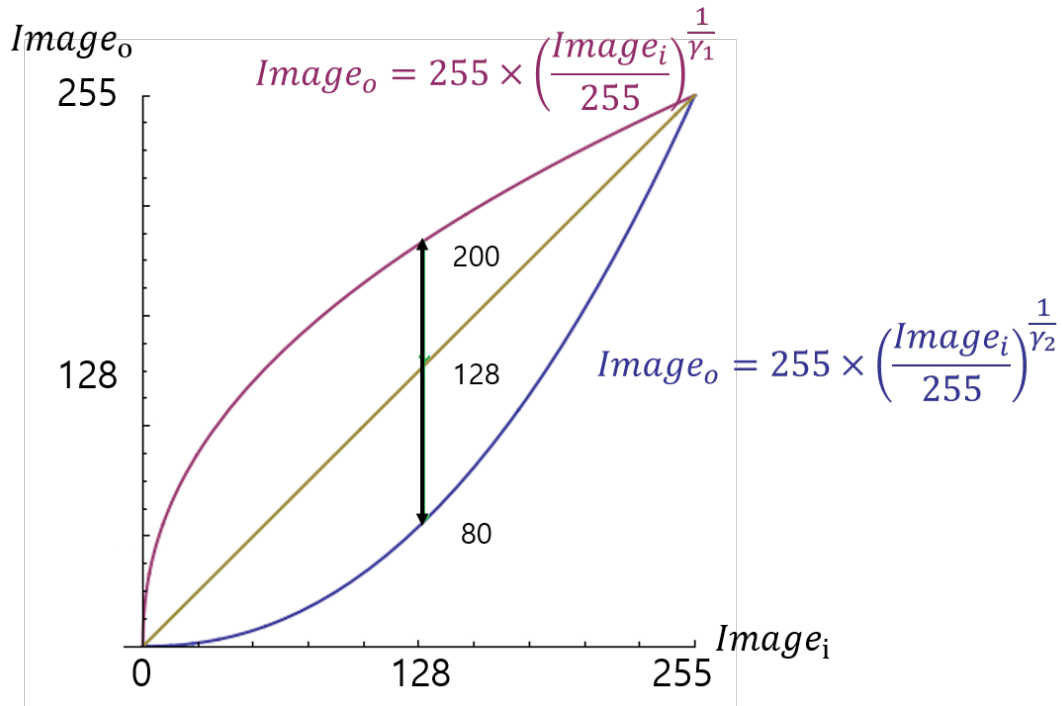


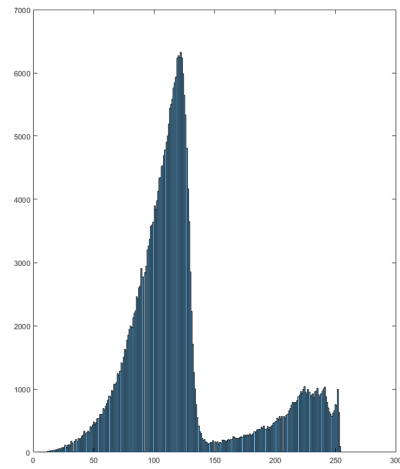
Figure 3.4: gamma function, $\gamma_1 > 1$, $0 < \gamma_2 < 1$.

Gamma transformation is an efficient function for converting images to dark or light in general, but it can be inappropriate if you want to change only a specific part. To solve this problem, there is a method of adjusting only a specific pixel using a conversion function set by the user. In Figure 3.6 (a), it is very cloudy and can not distinguish the subject. The result of this histogram conversion is shown in (b), which shows that there are two large peak points. γ_1 can be thought of as a background because of its relatively low pixel value, γ_2 can be thought of as a subject because of its relatively high pixel value. Therefore, γ_1 the peak should be made lower γ_2 must be made higher so that the subject can be clearly distinguished. In (d), the fraction less than γ_1 is mapped to a lower value because the slope is less than 1, The other area is mapped to a higher value because the slope is larger than 1. In (c), it can be seen that the background part becomes lower and the bright part becomes brighter.

Image enhancement using histogram transformation is not a universal approach. The reason is that it is difficult to predict what the histogram will look like in a very wide variety of situations. Nevertheless, the research fields that use this method are mainly those in which two classes are clearly distinguished in a situation where the brightness is constant. It is highly desirable to use the histogram transformation



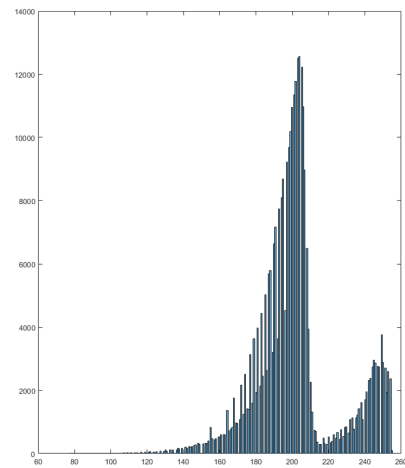
(a)



(b)



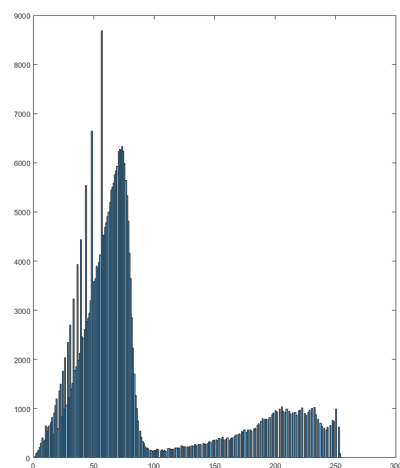
(c)



(d)



(e)

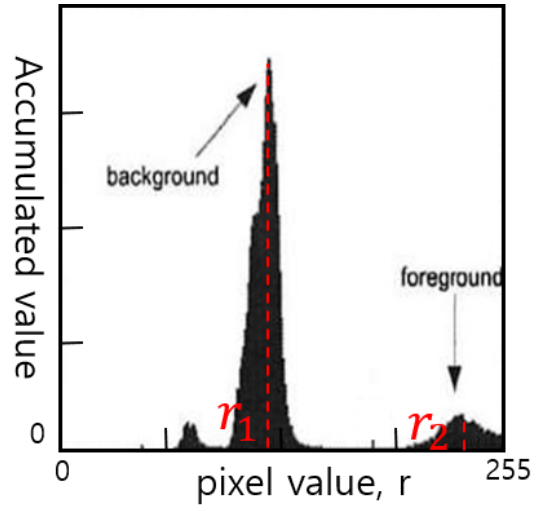


(f)

Figure 3.5: Gamma correction result, (a)-(b): Normal image, (c)-(d): Result of $\gamma = 0.5$, (e)-(f): Result of $\gamma = 1.5$.



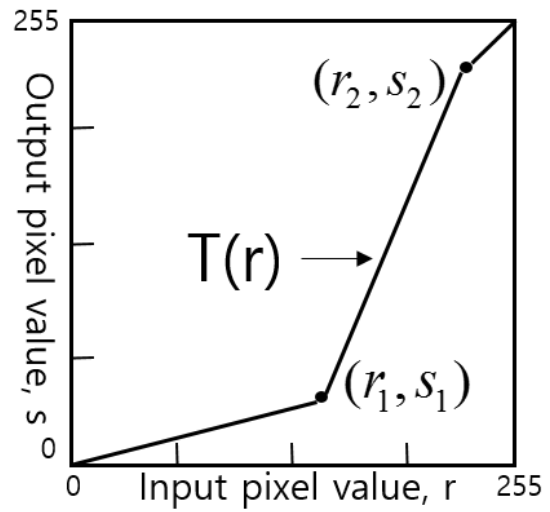
(a)



(b)



(c)



(d)

Figure 3.6: Histogram transformation, (a): Dark image, (b): Histogram transformation of (a), (c): Corrected image, (d): Transfer function

because the laser and the background in welding occur in two distinct classes: 'background' and 'laser'.

3.1.2 Image Enhancement using Spatial Filter

Image enhancement using a spatial filter is performed based on convolution. The 2D convolution is defined in the same way as 3.2.

$$\begin{aligned}
 y[m, n] &= h[m, n] * x[m, n] \\
 &= \sum_{j=-\infty}^{\infty} \sum_{i=-\infty}^{\infty} h[i, j] \cdot x[m-i, n-j] \\
 &= \sum_{j=-\infty}^{\infty} \sum_{i=-\infty}^{\infty} h_1[i] h_2[j] \cdot x[m-i, n-j] \\
 &= \sum_{j=-\infty}^{\infty} h_1[i] \cdot \sum_{i=-\infty}^{\infty} h_2[j] x[m-i, n-j]
 \end{aligned} \tag{3.2}$$

$$\begin{aligned}
 y[m] &= h[m] * x[m] \\
 &= \sum_{i=-\infty}^{\infty} h[i] \cdot x[m-i]
 \end{aligned} \tag{3.3}$$

Here, $y[m, n]$ represents results of convolution image, $x[m, n]$ represents input image, $h[m, n]$ represents kernel. It is clearly known that only difference between the second line of equation 3.2 and equation 3.3 is the dimension.

In order to clearly understand the image convolution in image processing, it is necessary to understand it through the picture. In Figure 3.7 (a) and (b) in refer to input image and kernel respectively. (c) shows the result at position [-1,-1], where $i = -1, j = -1$ in the expression 3.2. If you list it as a formula, it is expressed as 3.4. Generally, the outer range of the input image is calculated as 0 which is called zero-padding.

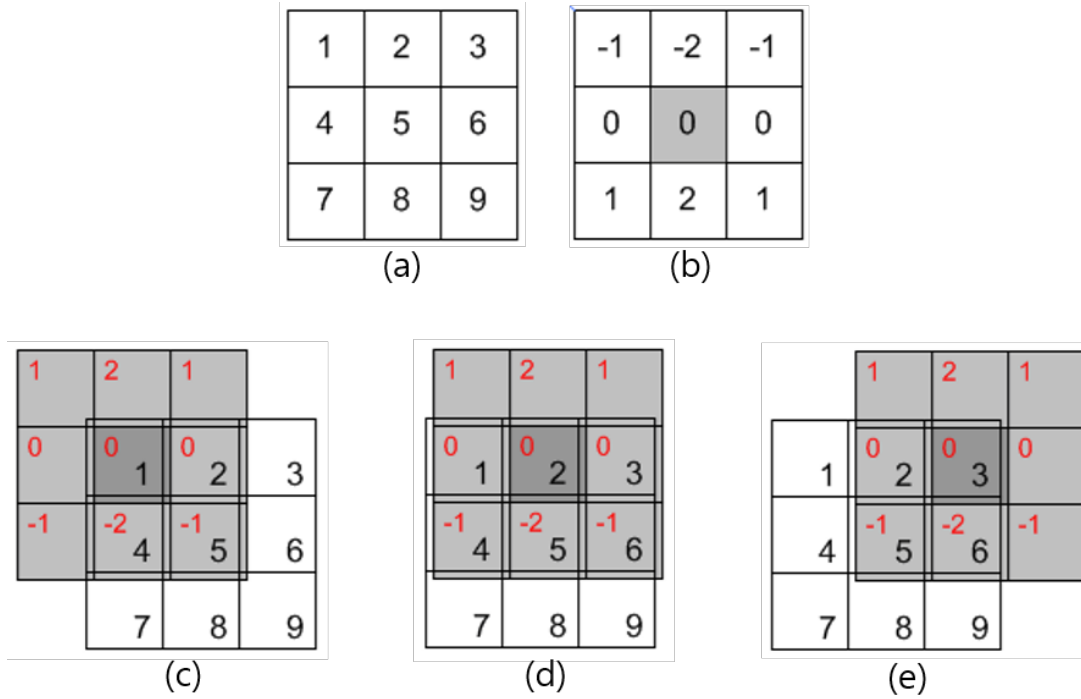


Figure 3.7: 2D convolution, (a): Input image, (b): kernel, (c): convolution result in $[-1,-1]$, (d): convolution result in $[0,-1]$, (e): convolution result in $[1,-1]$

$$\begin{aligned}
 y[-1, -1] &= x[-1, 1] \cdot h[1, 1] + x[0, 1] \cdot h[0, 1] + x[1, 1] \cdot h[-1, 1] + \\
 & x[-1, 0] \cdot h[1, 0] + x[0, 0] \cdot h[0, 0] + x[1, 0] \cdot h[-1, 0] + \\
 & x[-1, -1] \cdot h[1, -1] + x[0, -1] \cdot h[0, -1] + x[1, -1] \cdot h[-1, -1] \\
 &= 0 \cdot 1 + 0 \cdot 2 + 0 \cdot 1 + 0 \cdot 0 + 1 \cdot 0 + 2 \cdot 0 + 0 \cdot (-1) + 4 \cdot (-2) + 5 \cdot (-1) \\
 &= -13
 \end{aligned}
 \tag{3.4}$$

Filtering using convolution use the flipped kernel so it it no intuitive to understand. In image processing, cross-correlation is used for filtering to solve it. Cross-correlation is like convolution, except that it does not flip the kernel. I is define in equation 3.5. In general, filtering in an image means cross-correlation.

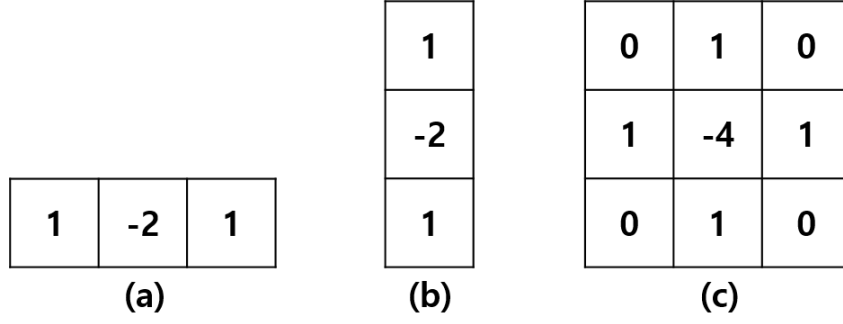


Figure 3.8: Laplacian kernel, (a): x-directional kernel, (b): y-directional kernel, (c): bi-directional kernel.

$$\begin{aligned}
 y[m, n] &= h[m, n] * x[m, n] \\
 &= \sum_{j=-\infty}^{\infty} \sum_{i=-\infty}^{\infty} h[i, j] \cdot x[m+i, n+j] \\
 &= \sum_{j=-\infty}^{\infty} \sum_{i=-\infty}^{\infty} h_1[i] h_2[j] \cdot x[m+i, n+j] \\
 &= \sum_{j=-\infty}^{\infty} h_1[i] \cdot \sum_{i=-\infty}^{\infty} h_2[j] x[m+i, n+j]
 \end{aligned} \tag{3.5}$$

Image filtering depends on which kernel using. Typically, the edge detection filter uses a Laplacian filter. The edge is where the pixel values change abruptly in the image. If you use a gradient that is a first order differential, you will only detect edges in one direction, so if you want to know the edges in all directions, use a second order differential(Laplacian).

$$\frac{\partial f}{\partial x} = f(x+1) - f(x) \tag{3.6}$$

$$\frac{\partial^2 f}{\partial^2 x} = f(x+1) + f(x-1) - 2f(x) \tag{3.7}$$

$$\nabla^2 f = \frac{\partial^2 f}{\partial^2 x} + \frac{\partial^2 f}{\partial^2 y} \tag{3.8}$$

$$\frac{\partial^2 f}{\partial^2 x} = f(x+1, y) + f(x-1, y) - 2f(x, y) \tag{3.9}$$

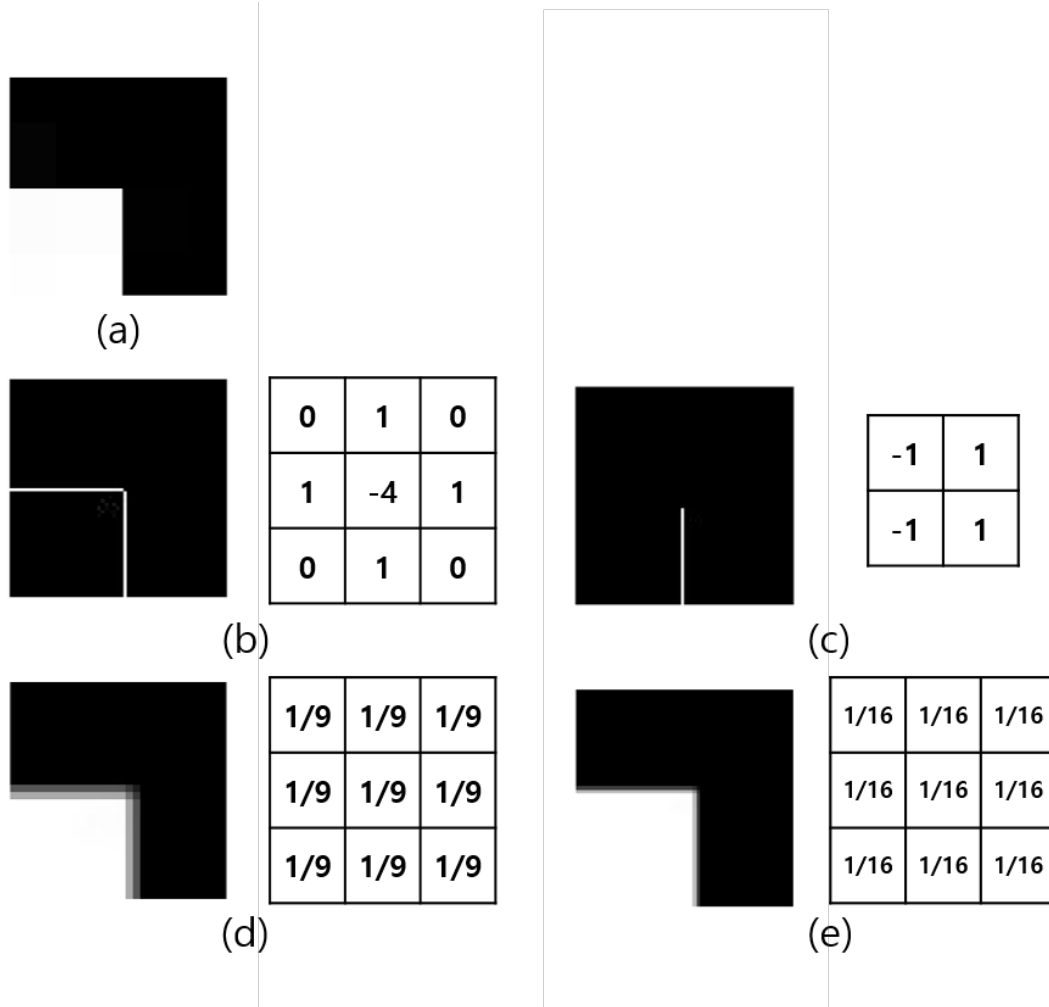


Figure 3.9: Kernels and results, (a): Original image, (b): Laplacian image, (c): Sobel image, (d): Mean image, (e): Gaussian image.

$$\frac{\partial^2 f}{\partial^2 y} = f(x, y + 1) + f(x, y - 1) - 2f(x, y) \quad (3.10)$$

$$\begin{aligned} \nabla^2 f = & [f(x + 1, y) + f(x - 1, y) \\ & + f(x, y + 1) + f(x, y - 1) \\ & - 4f(x, y)] \end{aligned} \quad (3.11)$$

Mathematically, the discrete first order differential is defined by the expression 3.6. Using this, we can express it as a second order differential equation 3.7. It can be expressed as 3.8 by Laplacian definition and 3.9 and 3.10 by using 3.7 to obtain each term. Therefore, the final result is the expression

ref eq: 3.11, which is represented by the picture 3.8. Equation 3.9 means the Figure 3.8 (a), equation 3.10 means 3.8 (b), equation 3.11 means 3.8 (c).

The result of filtering using this defined filter is shown in Figure 3.9. (a) is the original, (b) is the result of the edge filter, it detect all direction edges. (c) is a first-order differential filter, only one edge is detected. (d) is an average filter and the boundary value is blurred. (e) is the same in that the blur is performed with a Gaussian filter, but the weight of the kernel is more centered, and the tendency to maintain the edge is strong.

3.2 Background of Computer Vision[59]-[62]

Computer vision can be divided into geometric vision and pattern vision. The former aims at camera parameter estimation, distortion correction and attitude estimation starting from basic optics, and the latter is used mainly in the field of robotics such as detection, segmentation, and tracking. In this study, we used on the latter rather than the former. The application range of pattern vision is very different, but it is subjected to the same preprocessing process. It is image acquisition, image processing, and extracting feature points. Although there are various algorithms for each process, we focus on template matching used in this study.

3.2.1 Template Matching

If we want to obtain covariance or correlation in 1D signal processing, use convolution. In the image, correlation can be found in the image in a similar context. We use the above-mentioned cross-correlation and are called template matching. The result of (c) can be obtained by filtering the image 3.10 (a) with kernel (b). The brightest part in (c) becomes the most similar part to (a) in (b). Thus, if you want to see the similarity of a pattern in an image, you can use template matching.

There are many other ways. For example, [21] mentioned in the Chapter 2 was defined as 1.2. Most of the studies on weld line detection use basic filtering when using template matching or at a simple level such as RMS expression. This is because the difference between the template and the actual image is not large. There are many studies that use template matching in more difficult environments, but in

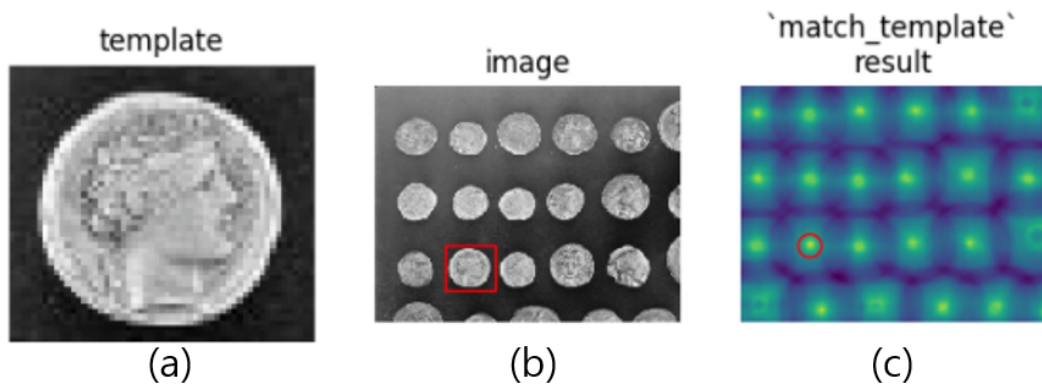


Figure 3.10: Template matching[62], (a): template image(kernel), (b): image, (c): filtering result

this study, we use a simple algorithm that is sufficiently detectable enough.

3.3 Process of Welding Line Detection

In this section, the detection algorithm of the weld line using the above-mentioned algorithm is explained in general. First, the welding line detection algorithm is as follows. The welding line detection algorithm consists of two major parts. The first is image quality enhancement and the second is weld line detection. Image quality enhancement aims at obtaining a robust image for seam detection. Weld line detection is an interesting goal to detect the image weld line through template matching to a good

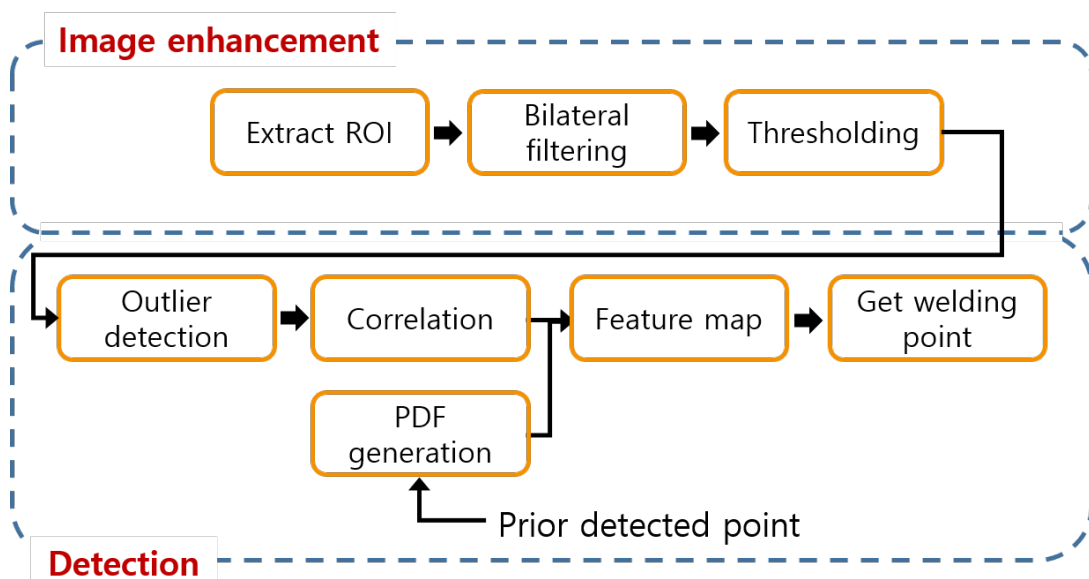


Figure 3.11: Welding line detection overall process flow

image refined through image processing.

3.3.1 Image Quality Enhancement

It is effective to obtain arc-insensitive image by using optical system, but it is hard to get the same level of image always due to the influence of reflected light, illumination of laboratory or weather when entering curved surface. Therefore, it is aimed to always obtain a similar level of image. Image processing is largely divided into four parts. (1) detection of the region of interest, (2) noise removal using smoothing, and (3) binarization.

The camera, laser and torch, designed as in Figure 2.15, are always in the same place. Therefore, the laser position of the image obtained through the camera is always constant, and the ROI can be extracted using this. Drawing 3.12 By extracting the ROI, the computation volume can be efficiently reduced, and the image processing can be performed by concentrating only the laser part, thereby reducing the bias caused by other parts.

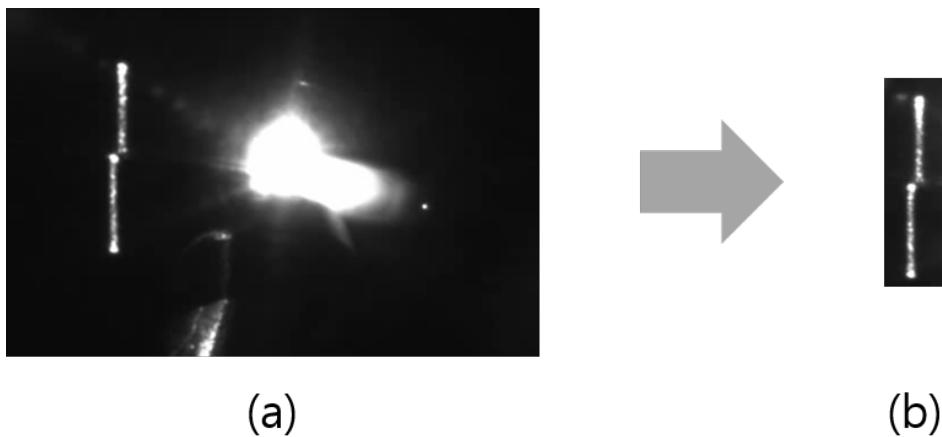


Figure 3.12: ROI extraction, (a): whole image, (b): ROI(Region of Interest)

The image obtained through the camera causes noise due to various reasons such as the amplification process of the electric signal and the interference of the ambient light. A blurring process is needed to remove this noise. In general blurring process, the edge component is not detected well, which causes the performance degradation of the detection part later. Therefore, we use a bilateral filter that preserves the edges. The bilateral filter is described in the figure 3.13. The difference between the pixel values

between the first and second columns and the difference between the second and third column pixel values in the leftmost figure in (a) is larger in the second and third columns. A column with a relatively larger difference is recognized as an edge and this part does not participate in the filtering process due to adjustment of the filter kernel value. Note that the kernel in Figure 3.13 (a) is defined as Gaussian and that all weights exist, but the kernel weight in (b) has no elements in column 3. As a result, (d) and (e), the edge is preserved and only the peripheral part is blurred.

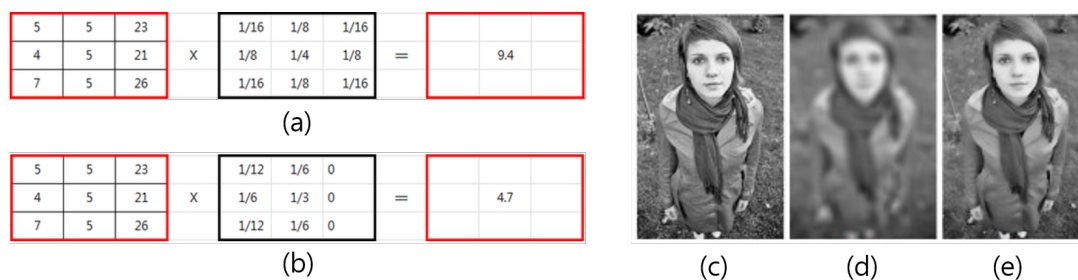


Figure 3.13: Bilateral filtering, (a): Gaussian filter kernel, (b): bilateral filter kernel, (c): original image, (d): blurred image using Gaussian filter, (e): blurred image using bilateral filter

The next step is the thresholding process. Generally, thresholding is set to 0 if the user sets a value at random and the value is set to 1 if it is not exceeded. This method has difficulty setting different values according to the situation. Most of the thresholding recently uses Otsu's method. Otsu's method sets the thresholding value by using the result of the peak value between classes in the result of the histogram (b) when there are two class images like figure 3.14 (a). As a result, a refined image (c) can be obtained. The Figure 3.15 (a) is original image, (b) is result of blurring of ROI, (c) is thresholding by Otsu's method thresholding with image enhancement (d) is thresholding by Otsu's method thresholding without image enhancement. As (c), (d) results show, image enhancements has a great role.

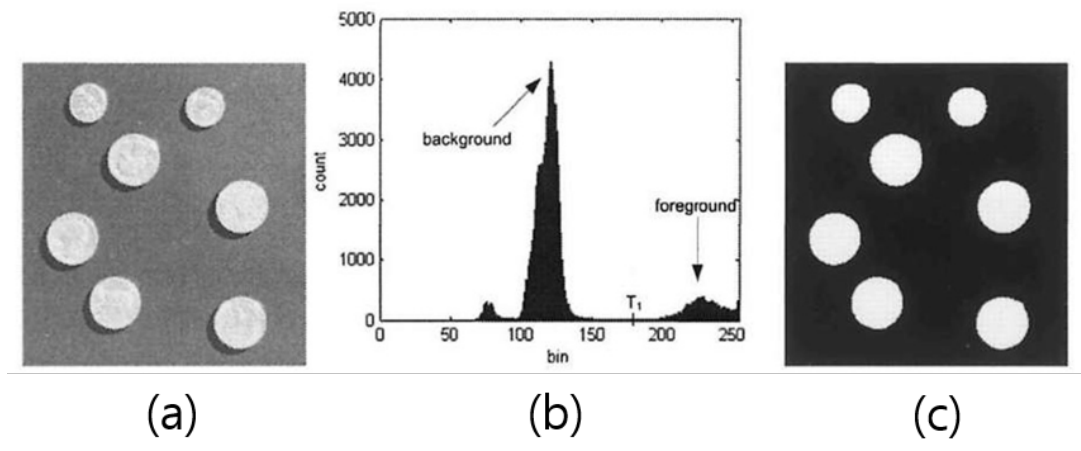


Figure 3.14: Otsu's binarization, (a): original image, (b): bi-modal histogram, (c): result.

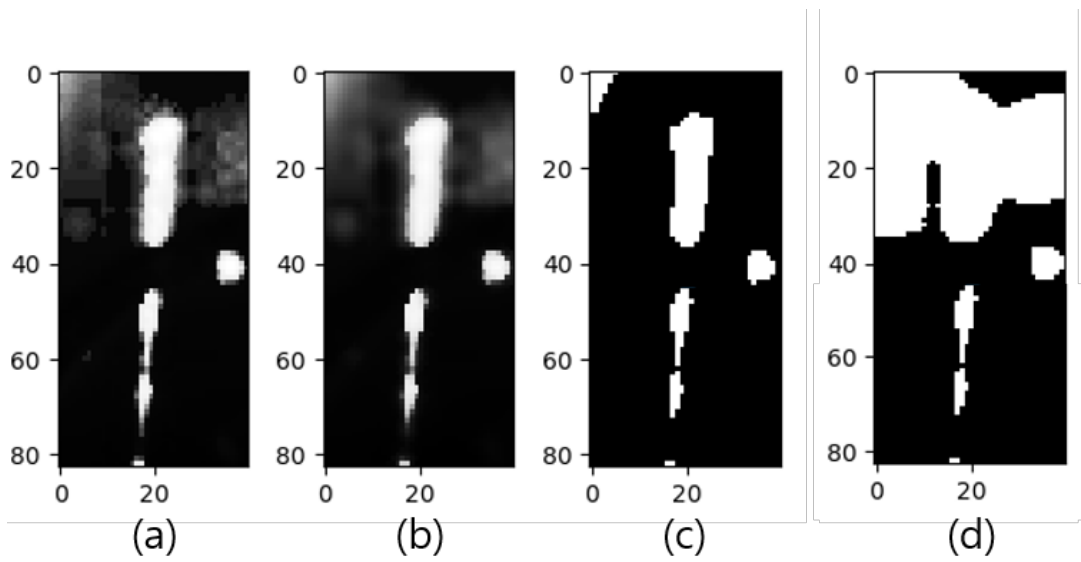


Figure 3.15: Results of image enhancement, (a): original image, (b): blurred image, (c): thresholds with image enhancement, (d): thresholds without image enhancement.

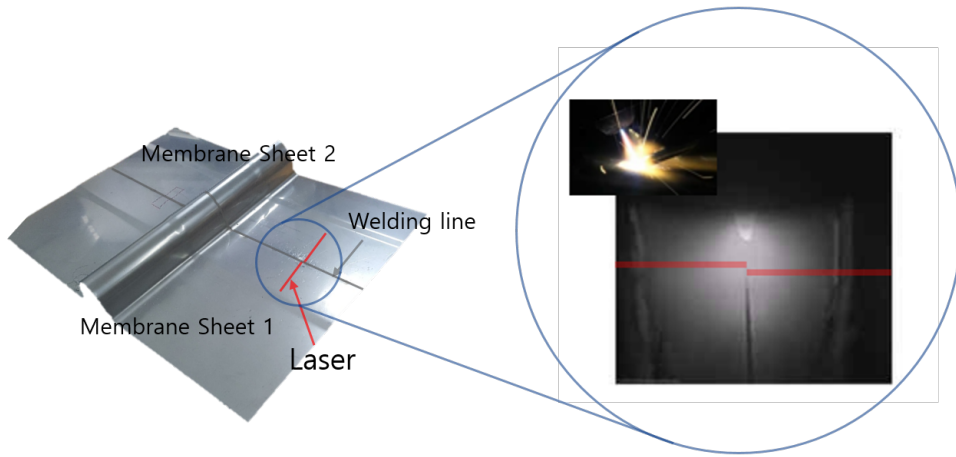


Figure 3.16: Laser geometry.

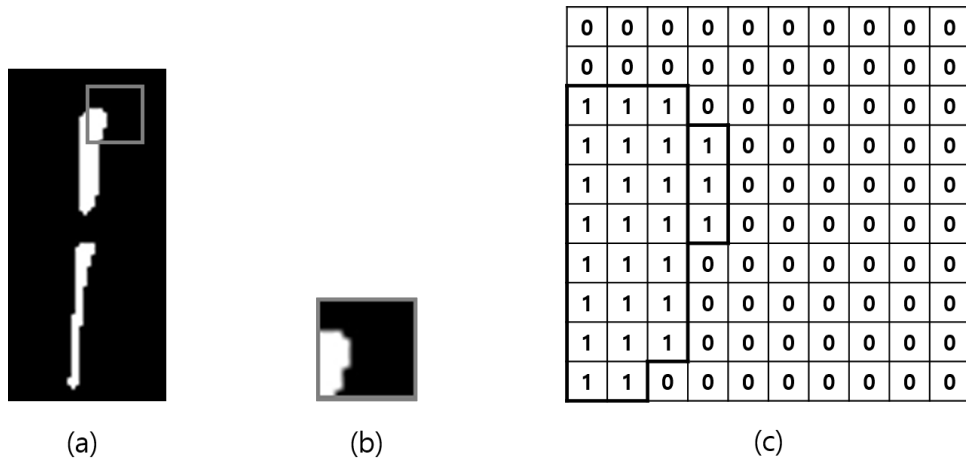


Figure 3.17: Binarization image, (a): whole ROI image, (b): closed-up image, (c): real-data table.

3.3.2 Welding Line Detection

Weld line detection is roughly divided into two types. The first step is feature point extraction and the next step is tracking. In the figure 3.11, the parts corresponding to feature extraction are a correlation, probability density function (PDF) generation, probability block, and the tracking step is the outlier detection and get welding point. The outlier detection is explained in tracking step even if it process very beginning.

Understanding the detail extraction step requires some background knowledge. Welding is the work of melting one of the two steel materials and joining them together. As shown in figure 3.16, two overlapping parts of steel are welded together, resulting in a step difference in the weld line due to the

difference in height between two steel parts. At this time, when the laser beam is irradiated on the weld line, a discontinuity point is created between the upper steel part and the lower steel part by the step difference. At that time, the point where the discontinuity point occurs based on the steel material is the welding point.

The Figure 3.17 (a) shows the binarized image in image processing. (B) is a partial enlargement of a specific region which is a gray region. If you look at this part in an actual table, it looks like (c). The laser part is higher than the threshold value and displayed as 1, and other background parts are displayed as 0. Now, the goal is to detect the part where the step is formed in this part. It is possible to use the template matching described above in advance, but an over-matching problem of template matching occurs.

The figure 3.18 illustrates the over-matching problem. (a) is an arbitrary table and (c) is an image

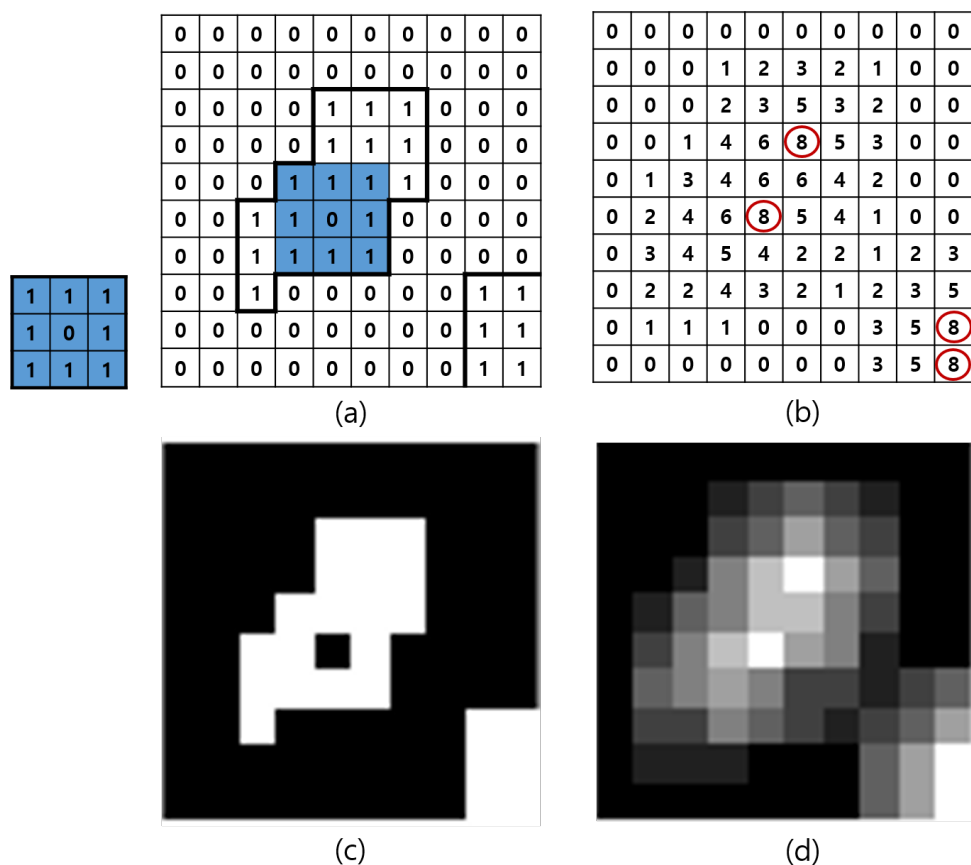


Figure 3.18: Template matching, (a): kernel and original image table, (b): matching result with several peaks, (c): original image, (d): matching result image.

0	0	0	0	0	0	0	0	0	0	0	0	0
0	0	0	0	0	0	0	0	0	0	0	0	0
0	0	0	0	0	0	0	0	0	0	0	0	0
0	0	0	0	1	1	1	0	0	0	0	0	0
0	0	0	0	1	1	1	0	0	0	0	0	0
0	0	0	1	1	1	1	0	0	0	0	0	0
0	0	1	1	0	1	0	0	0	0	0	0	0
0	0	1	1	1	1	0	0	0	0	0	0	0
0	0	1	0	0	0	0	0	1	1	1	1	1
0	0	0	0	0	0	0	0	1	1	1	1	1
0	0	0	0	0	0	0	0	1	1	1	1	1
0	0	0	0	0	0	0	0	1	1	1	1	1
0	0	0	0	0	0	0	0	1	1	1	1	1
0	0	0	0	0	0	0	0	1	1	1	1	1

Figure 3.19: Symmetric padding .

obtained by imaging it. At this time, symmetric padding like 3.19 was used to padding to maintain image size. In (a), the blue area is defined as the kernel, and template matching is performed to obtain the figure (b), and the normalized image based on the maximum value is drawn as (d). (c) is the maximum value, and the points are considered to be similar to the kernel. Therefore, even if it is similar to the original shape, the same score as the picture to be detected is obtained. Thus, the uncertainty increases significantly, which leads directly to a lower detection rate.

In order to prevent it, we solve this problem by simply defining zero elements of kernel as -1. The result is illustrated in the figure 3.20. Note that (a) the 0 component of the kernel changes to -1 when compared to 3.18 (a). (b) is a template matching result table, and (d) is a its figure. The over-matching problem was easily solved by simple numerical manipulation.

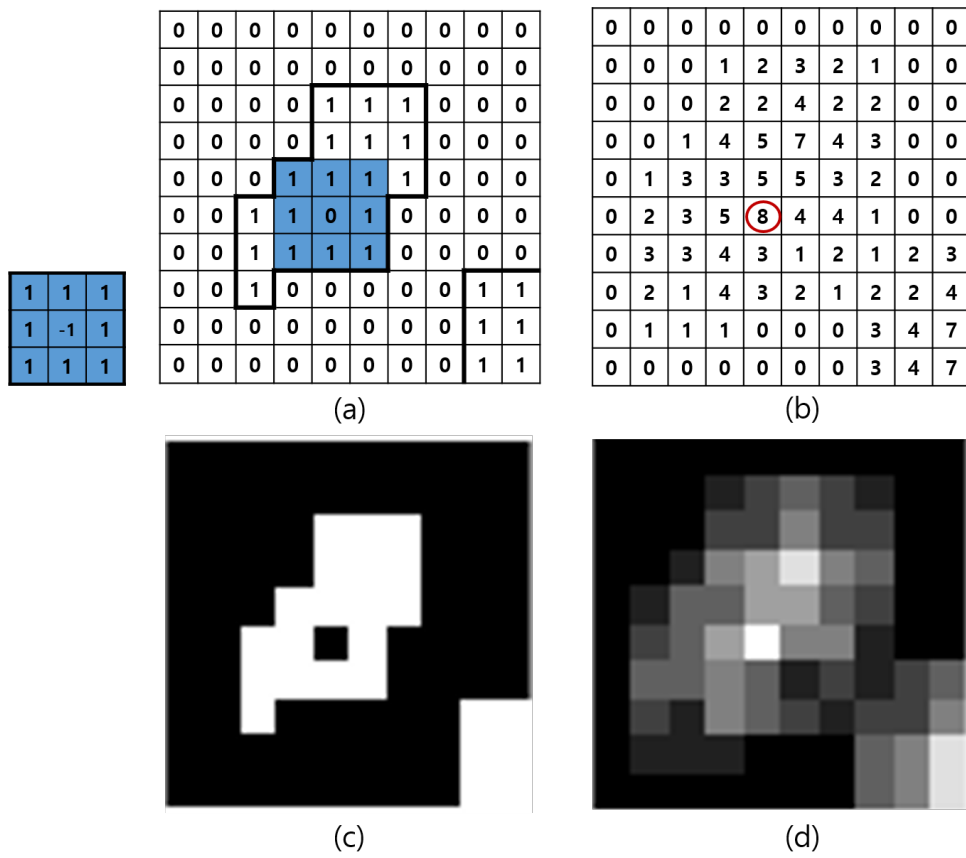


Figure 3.20: template matching with modified kernel, (a): kernel and original image table, (b): matching result with several peaks, (c): original image, (d): matching result image .

The figure 3.21 shows the process of performing template matching on this modified kernel. The Figure 3.21 (a) is a pre-defined image, defining the weld point and defining the kernel as shown in (b). (c) shows the image processed by each frame and (d) is the result of template matching. The white spot has the highest value and matches the actual weld point.

The Figure 3.21 (a) is a predefined image. In (a), we define the welding point and generate the kernel as shown in (b). (c) shows the image processed by each frame and (d) is the result of template matching. The white spot has the highest value and matches the actual weld point.

The figure 3.22 is a second-order Gaussian probability model with mean and variance. The assumptions for introducing the Gaussian probability model are as follows. Since the vibration experienced by the actual mechanical system enters in the form of noise in the natural world, the detection points of the previous frame and the current frame follow the Gaussian distribution based on the detection point of the previous frame. Therefore, the probability that a welding spot exists at each position in the current frame is affected by the previous frame. Here, the average uses the detection point of the previous frame, the variance is fixed but it is modified to reflect the previous detection history, it is explained in detail in the tracking section. The figure 3.23 illustrates the overall process. (a) is the kernel, (b) is the result of template matching, (c) is the Gaussian model-based probability density function, (d) is the result of the elements wise product of (b) feature point. The feature is a probability defined by the welding point, and the higher the probability is, the closer it is to judge the welding point.

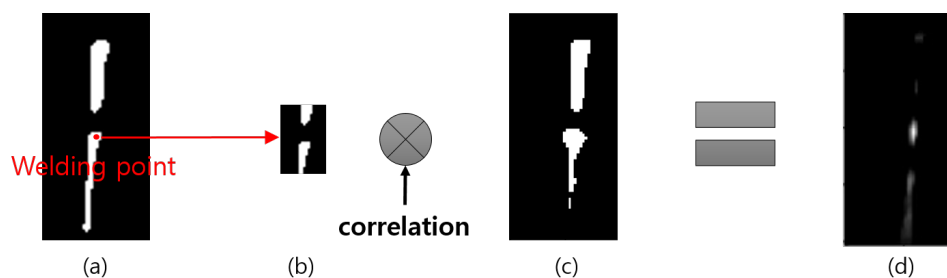


Figure 3.21: template matching process and result of image, (a): pre-defined image, (b): pre-defined kernel, (c): input image, (d) result of template matching.

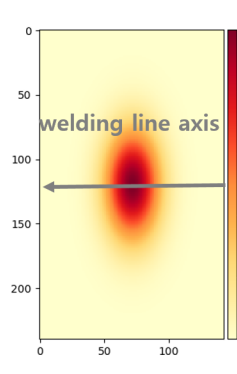


Figure 3.22: probability density fuction

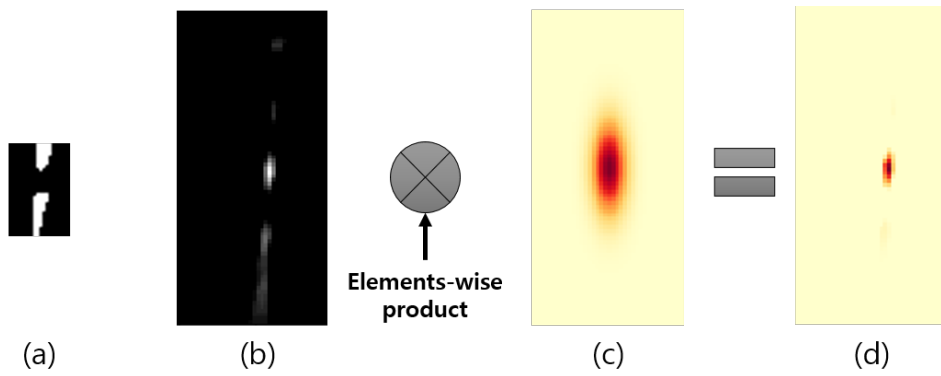


Figure 3.23: Feature point map generation process, (a): kernel, (b): template matching result, (c): PDF, (d): feature point map

Next, outlier detection and numerical filters are required. Since outlier detection is based on thresholding image, it proceeds in the order of precedence but is strictly included in the tracking step.

Outliers are caused by points created to fix steel temporarily before welding. This can be seen in the figure 3.24. (b) is an image obtained through a camera when a laser is irradiated on a steel in general. (c) is an image obtained by the laser through the camera when an outlier exists, and it can be confirmed that light is scattered greatly. (d) is a figure drawn the line on (b) detected using the Hough transform. (e) is a drawing drawn on (c) of a straight line detected using Hough transform. (d) and (e), it can be seen that the number of straight lines detected due to scattering of light is significantly different. Therefore, the outlier can be detected primarily as a result of the hough transform.

The figure 3.25 (a) shows the result of the straight line and binarized image detected through Hough transform. (b) is a drawing of only the linear component of the laser obtained through the Hough transformation of the outlier image. Due to scattering of light, the step for detecting the weld line is not visible at all in (b). This causes a difference in the number of bright color pixels on the straight line detected by the Hough transform. (c) is a the figure in which the same motion is repeated for the entire moving sequence. In (c), if the value is above or below a certain level, it can be detected as outlier.

The above process is summarized again as the figure 3.26. First, Hough transform on the binarized image. If the number of straight lines detected by the Hough transform is one, the process proceeds to the next step. Pixel counting is performed on one straight line to confirm whether it meets a predetermined range. If it passes, it is classified as normal image, and if one is not satisfied, it is classified as outlier image.

In the final get welding point step, a second-order FIR filter was designed for numerical compensation. The parameter coefficients were set using the results of linear fitting of true values.

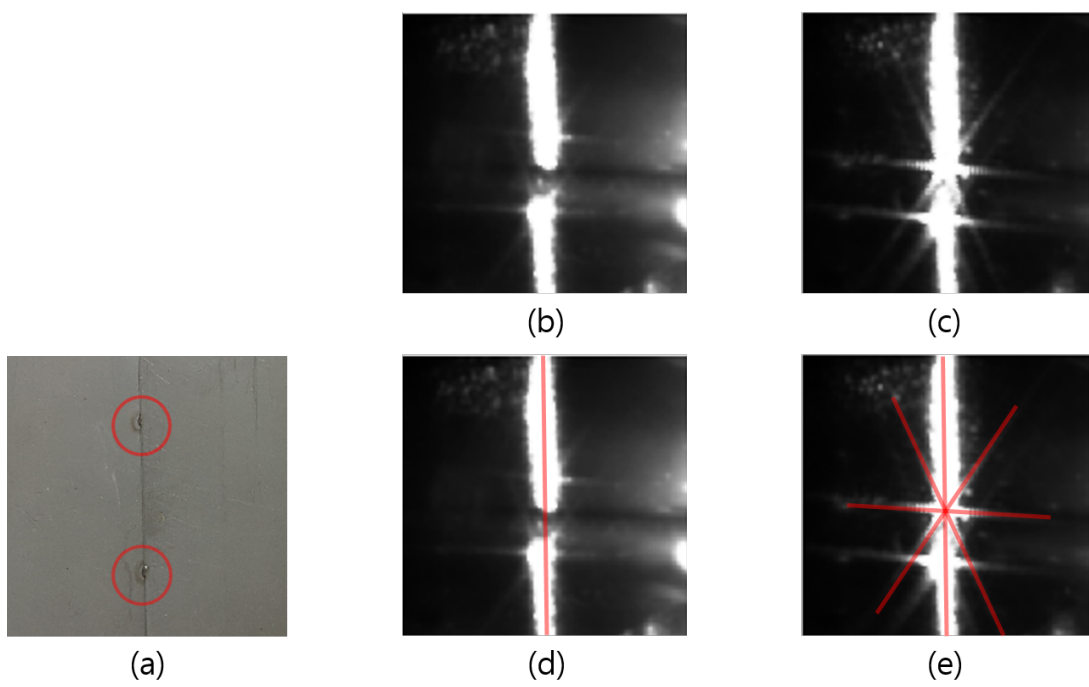


Figure 3.24: Outlier image, (a): pre-welded point, (b): normal laser raw image, (c): outlier laser raw image, (d): normal laser raw image with Hough transform result, (e): outlier laser raw image with Hough transform result

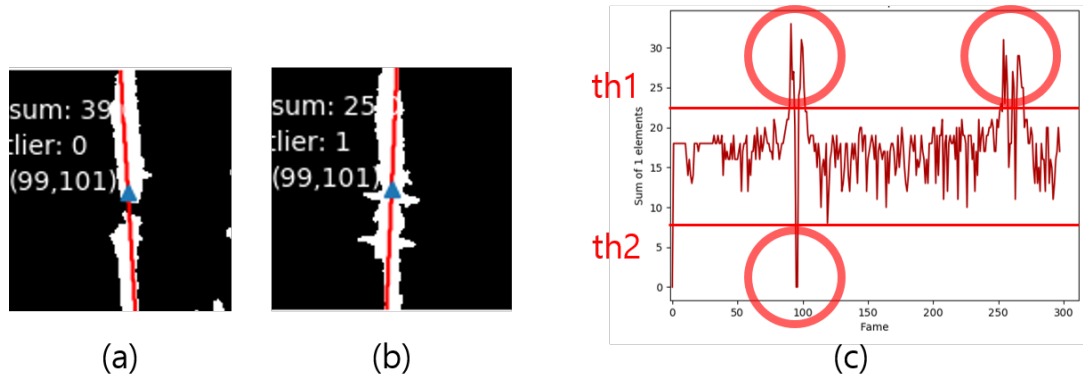


Figure 3.25: Outlier detection, (a): normal image with Hough transform result, (b): outlier image with Hough transform result, (c): pixel-counting result

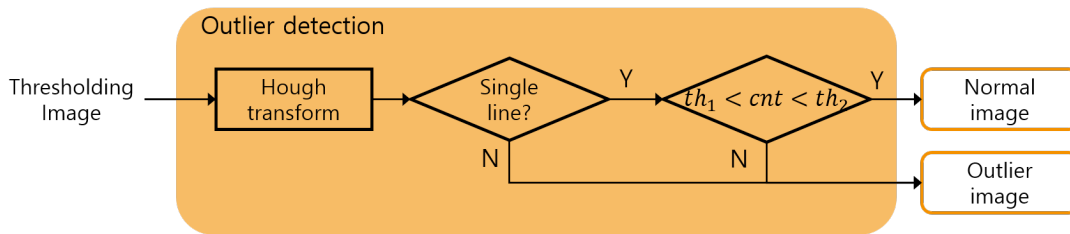


Figure 3.26: Summary of outlier detection

3.4 Results

The figure 3.27, the figure 3.28 and the table 3.4 show the results of the detection algorithm. All the horizontal axes of the figure ref fig3.27 and the figure ref fig3.28 are the frame order and the vertical axis is the pixel coordinates of the X component or Y component in detection. The X component is a axis parallel to the weld line, and the Y component is a component parallel to the laser. The vertical axis is about 50 mm, which change to about 4 mm.

The figures (a) and (b) in the figure 3.27 are the results of X and Y axes, respectively, when all the algorithms are applied. X is a frame determined to be outlier at the time of detection. (c) and (d) are graphs with outlier detection removed among the entire algorithm. 3.28 (a) and (b) are graphs with the kernel removed. Finally, (c) and (d) are the results without PDF generation.

The graph above is quantitatively computed and summarized in the table 3.4. When all algorithms are applied, the RMS error is 0.17mm and the peak error does not exceed 1mm. This is a value that

meets the target RMS error of 0.2mm and is much better than the error level of 1 1.5mm which is actual welder regarding as bad welding. In addition, when the outlier detection or modifying kernel is removed, the RMS y-axis error is not very good and the peak error has a performance much higher than 5mm. If the PDF generation is removed, it can not be detected.

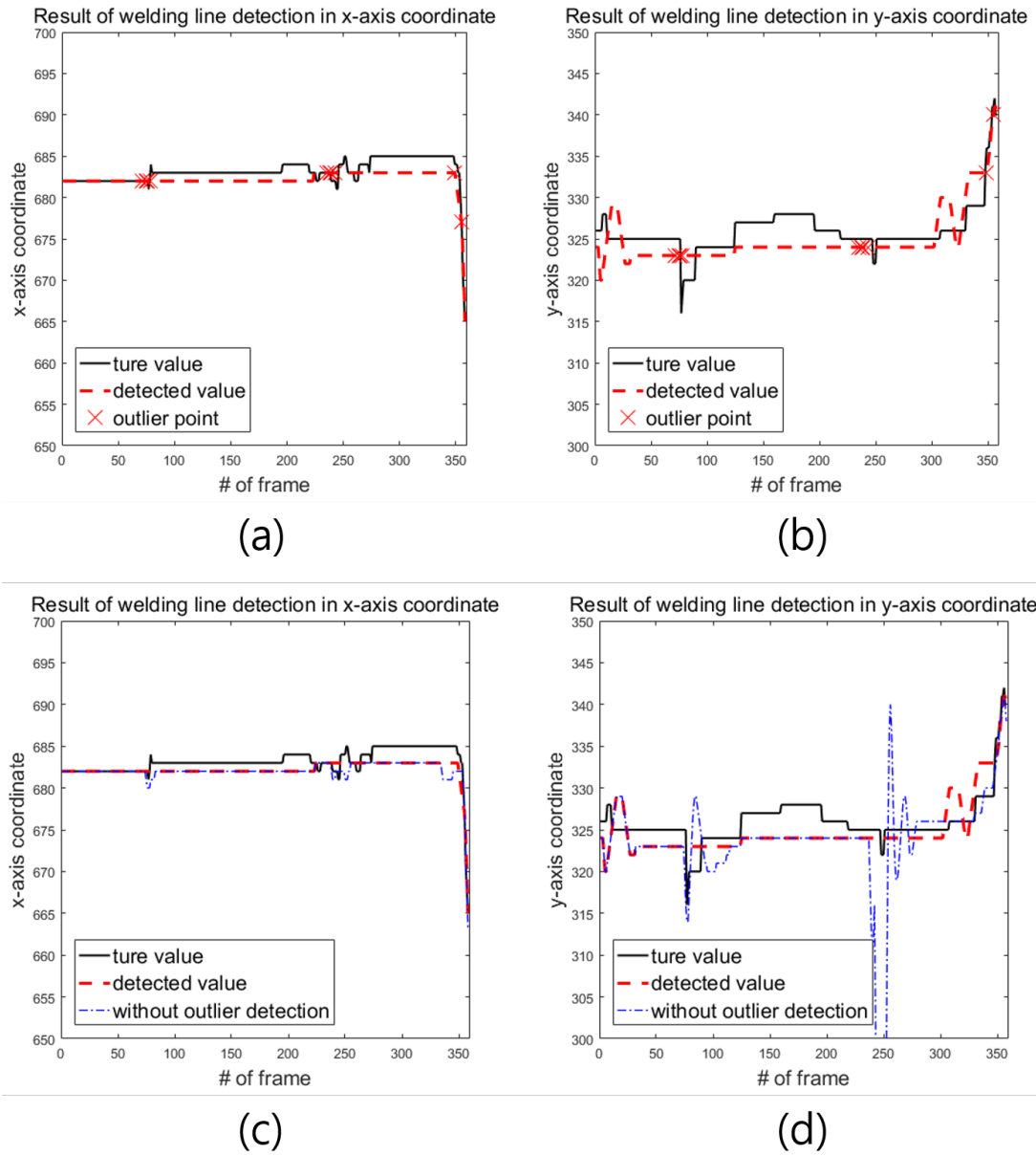


Figure 3.27: Welding line detection result 1, (a): X-axis result of Full algorithm, (b): Y-axis result of full algorithm, (c): X-axis result of excepting outlier detection, (d): Y-axis result of excepting outlier detection

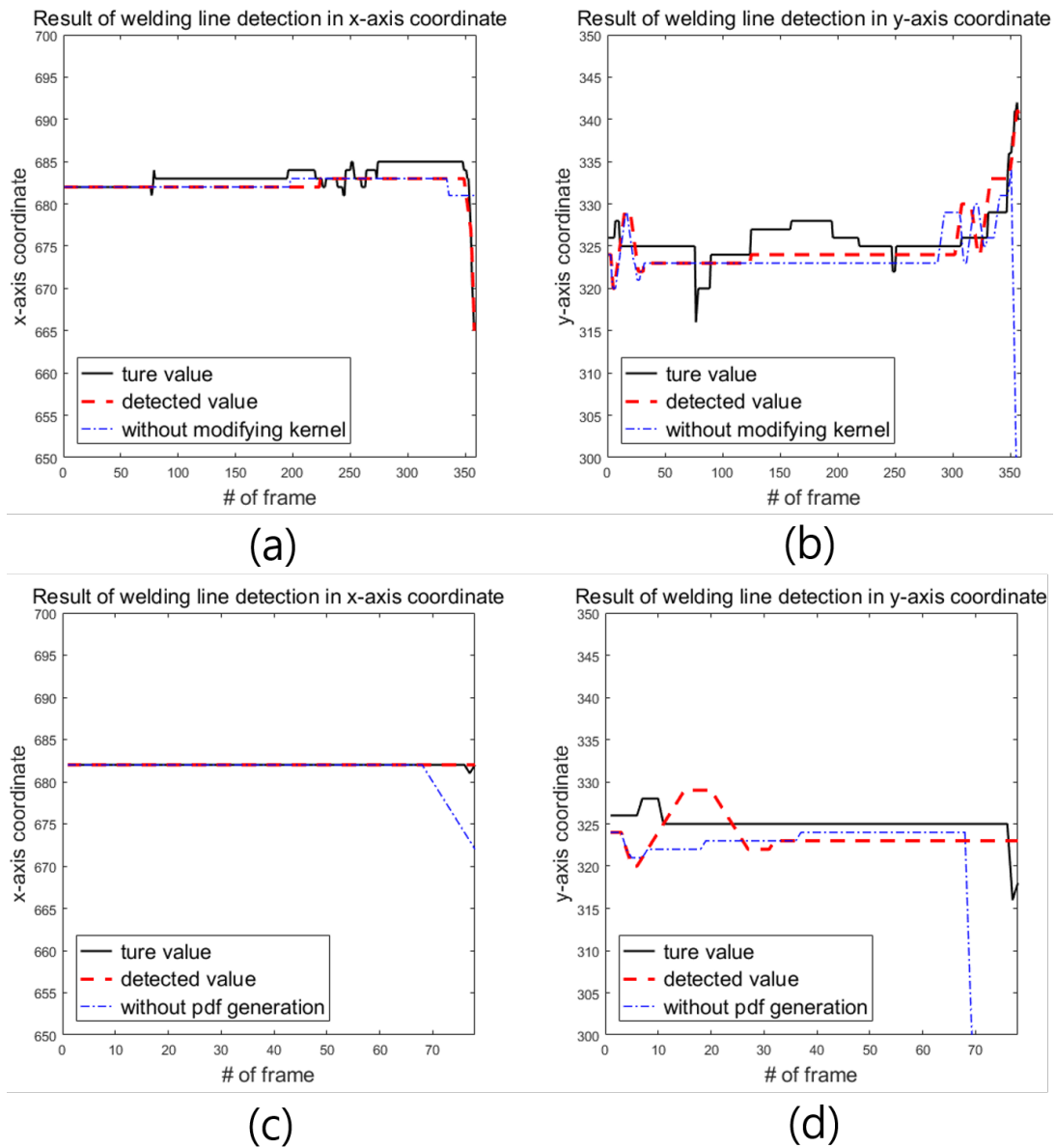


Figure 3.28: Welding line detection result 2, (a): X-axis result of excepting modifying kernel, (d): Y-axis result of excepting modifying kernel, (c): X-axis result of excepting PDF generation, (d): Y-axis result of excepting PDF generation

Table 3.1: Welding line detection result, the table result is shown comparison between 905nm and 980nm, without outlier detection, modifying kernel and PDF generation.

	Algorithms	RMS error		Peak error		
		X [mm]	Y [mm]	X [mm]	Y [mm]	
905nm system	Full algorithms	0.17	0.34	0.63	1.68	
	Full algorithms	0.11	0.17	0.33	0.58	
	outlier detection	0.12	0.79	0.34	5.8	
980nm system	Without	modifying kernel	0.16	0.55	1.3	5.2
		pdf generation	Detection fail			

Chapter 4. Conclusion and Future Works

4.1 Conclusion

In this paper, we propose a method to create a weld line detection vision algorithm for fully automated welding robots. The existing welding line detection method does not effectively remove the interference to the arc and deals only with the detection in the case where the welding does not proceed. This semi-automatic welding method is not fully automated because it can not effectively increase the working efficiency and still rely on the monitoring. Therefore, heavy industry companies are reluctant to apply them.

To solve this problem, the optical system using spectral analysis was applied to reduce the influence on the arc effectively. The results showed that the arc-to-laser power ratio was 0.4% in the absence of the optical system, but increased to 89% in the 980nm optical system. Therefore, without heavy image processing, we can obtain detectable laser image.

A template matching based method was used to detect the welding line. This is the most reasonable method for detecting the weld line because the mark is generated in real time due to the step difference when irradiating the laser. Also, outlier detection and numerical filters are added to the algorithm for exception handling. The result is 0.17mm in RMS value which is better performance than the goal RMS error value of 0.2mm. In addition, better than 1 1.5mm error level which is judged as bad welding in actual manual welding.

4.2 Future works

In the case of the membrane sheet, which is the target in this paper, the curved surface and the flat surface exist simultaneously. However, since the current design of the robot can not be changed as shown in the figure 2.14, it has a mechanical limitation. Specifically, when looking at the figure 4.1, as in (a), the laser enters the angle of view of the camera perfectly. (b) is a diagram illustrating the divided

regions of the flat and the curved parts. (c), it can be observed that as the welding torch gradually enters the curved portion, the laser band gradually disappears from the view point. (d), it can be seen that it is completely out of view point and only one side is visible.

Detecting these mechanical limitations by making the detection algorithm a little more adaptive to the case, we decided that there will be a problem in detection in applying to various steel materials in the future. Therefore, it is considered that it is best to reduce the mechanical interference in the process of redesigning the automatic welding robot since the arc effect is insufficient using the optical system. In summary, the contents of robot redesign considering angle of view are added in future studies.

In addition, there remains a need to determine the best fit of the seam detection algorithm and hardware development for sensor development.

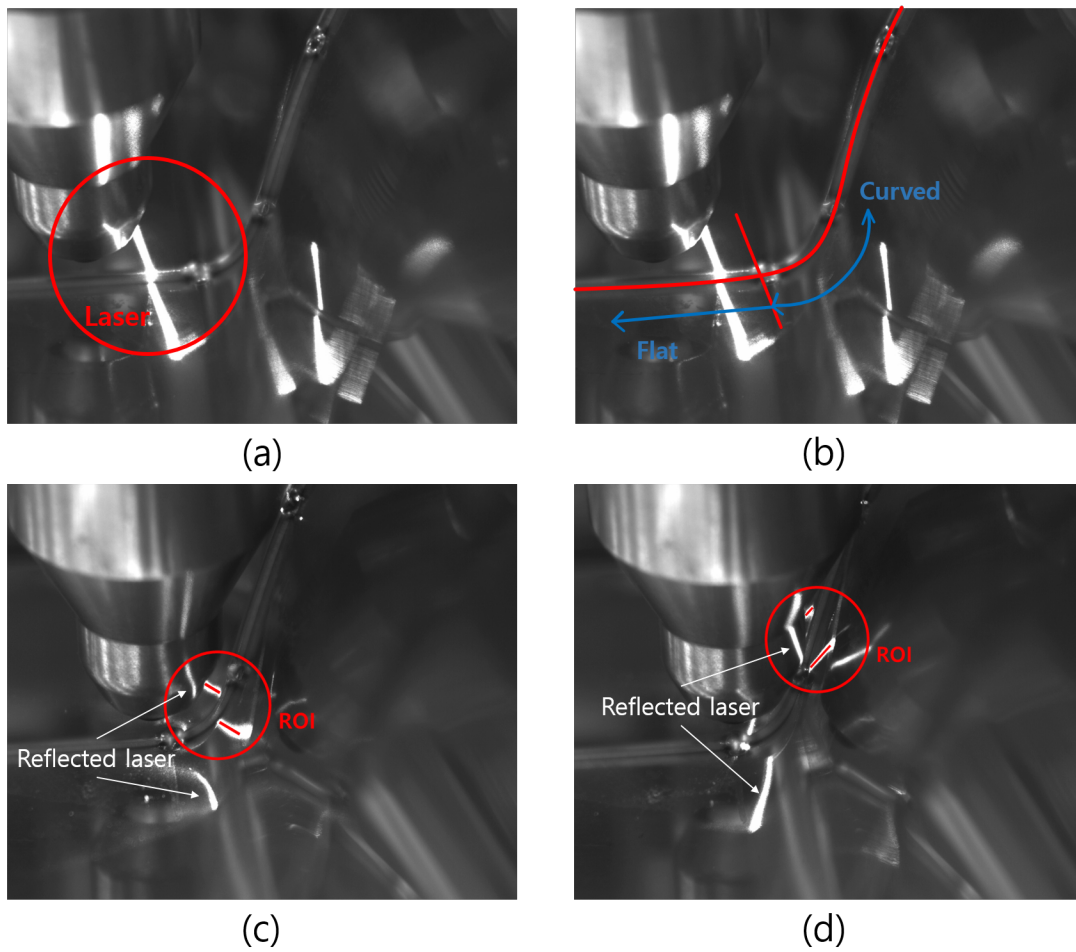


Figure 4.1: Vanishing view point problems, (a): Laser in the flat region, (b): Description of the flat and curved region, (c): Entering the curved region, (d): Vanishing view point in the curved region

Bibliography

- [1] Ogawa, Y., *Visual Analysis of Welding Processes, in Welding Processes*, Technical report, Intech corp., 2016.
- [2] Andersen, K., et al., "title," *Artificial neural networks applied to arc welding process modeling and control*, vol. 179, pp. 824-830, date. 1990
- [3] Lu, F., et al., "Modeling and finite element analysis on GTAW arc and weld pool," *Computational Materials Science*, vol. 29, pp. 371-378, date. 2004
- [4] Choo, R., J. Szekely, and R. Westhoff, "On the calculation of the free surface temperature of gas-tungsten-arc weld pools from first principles: Part I. Modeling the welding arc," *Metallurgical Transactions B*, vol. 23, pp. 357-369, 1992.
- [5] Valensi, F., et al., "Plasma diagnostics in gas metal arc welding by optical emission spectroscopy," *Journal of Physics D: Applied Physics*, vol. 43, pp. 434002, 2010.
- [6] Wu, C., T. Polte, and D. Rehfeldt, "Gas metal arc welding process monitoring and quality evaluation using neural networks," *Science and technology of welding and joining*, vol. 5, pp. 324-328, 2000.
- [7] Alfaro, S.C., D.d.S. Mendonça, and M.S. Matos, "Emission spectrometry evaluation in arc welding monitoring system," *Journal of Materials Processing Technology*, vol. 179, pp. 219-224, 2006.
- [8] Jia, C., et al., "Spectroscopic analysis of the arc plasma of underwater wet flux-cored arc welding," *Journal of Materials Processing Technology*, vol. 213, pp. 1370-1377, 2013.
- [9] Yu, H., et al., "Arc spectral processing technique with its application to wire feed monitoring in Al-Mg alloy pulsed gas tungsten arc welding," *Journal of Materials Processing Technology*, vol. 213, pp. 707-716, 2013.

- [10] Zhang, Z., et al., "Real-time defect detection in pulsed GTAW of Al alloys through on-line spectroscopy," *Journal of Materials Processing Technology*, vol. 213, pp. 1146-1156, 2013.
- [11] Mirapeix, J., et al., "Defect detection with CCD-spectrometer and photodiode-based arc-welding monitoring systems," *Journal of Materials Processing Technology*, vol. 211, pp. 2132-2139, 2011.
- [12] Zhang, L., et al., "Robust weld line detection with cross structured light and Hidden Markov Model," in *International Conference on Mechatronics and Automation (ICMA)*, , pp. 1411-1416, 2012 .
- [13] Wang, Y., et al., "Detection of line weld defects based on multiple thresholds and support vector machine," *NDT & E International*, vol. 41, pp. 517-524, 2008.
- [14] Carvalho, E.A., et al., "Fault-tolerant weld line detection for automatic inspection of storage tanks based on distance and visual information fusion," in *Instrumentation and Measurement Technology Conference*,, pp. 791-796, 2009.
- [15] Sun, J.-D., et al., "Welding seam detection and feature point extraction for robotic arc welding using laser-vision," in *International Conference on Ubiquitous Robots and Ambient Intelligence (URAI)*,, pp. 644-647, 2016 .
- [16] Wang, Z., "Unsupervised Recognition and Characterization of the reflected Laser Lines for Robotic Gas Metal Arc Welding," *IEEE Transactions on Industrial Informatics*, vol. 13, pp. 1866 - 1876, 2017.
- [17] Usamentiaga, R., J. Molleda, and D.F. García, "Fast and robust laser stripe extraction for 3D reconstruction in industrial environments," *Machine Vision and Applications*, vol. 23, pp. 179-196, 2012.
- [18] Zhang, L., et al., "A novel laser vision sensor for weld line detection on wall-climbing robot," *Optics & Laser Technology*, vol. 60, pp. 69-79, 2014.

- [19] Zhang, L., et al., "Weld line detection and tracking via spatial-temporal cascaded hidden Markov models and cross structured light," *IEEE Transactions on Instrumentation and Measurement*, vol. 63, pp. 742-753, 2014.
- [20] Dinham, M. and G. Fang, "Detection of fillet weld joints using an adaptive line growing algorithm for robotic arc welding," *Robotics and Computer-Integrated Manufacturing*, vol. 30, pp. 229-243, 2014.
- [21] Wenjie, C.X.Z.Z.C, "VISION-BASED RECOGNITION AND GUIDING OF INITIAL WELDING POSITION FOR ARC-WELDING ROBOT," *Chinese Journal of Mechanical Engineering*, vol. 18, pp. 1.
- [22] Dinham, M. and G. Fang, "Autonomous weld seam identification and localisation using eye-in-hand stereo vision for robotic arc welding," *Robotics and Computer-Integrated Manufacturing*, vol. 29, pp. 288-301, 2013.
- [23] Liu, J., et al., "A real-time passive vision system for robotic arc welding," in *IEEE International Conference on Automation Science and Engineering (CASE)*, pp. 389-394, 2015.
- [24] Yang, S.-M., et al., "Weld line detection and process control for welding automation," *Measurement Science and Technology*, vol. 18, pp. 819-826, 2007.
- [25] Molina, L., et al., "A robotic vision system using a modified Hough transform to perform weld line detection on storage tanks," in *IEEE Latin American Robotic Symposium*, pp. 45-50, 2008.
- [26] Ballard, D.H., "title," *Generalizing the Hough transform to detect arbitrary shapes. Pattern recognition*, vol. 13, pp. 111-122, 1981.
- [27] Xu, L., E. Oja, and P. Kultanen, "A new curve detection method: randomized Hough transform (RHT)," *Pattern recognition letters*, vol. 11, pp. 331-338, 1990.
- [28] Kiryati, N., Y. Eldar, and A.M. Bruckstein, "A probabilistic Hough transform," *Pattern recognition*, vol. 24, pp. 303-316, 1991.

- [29] Illingworth, J. and J. Kittler, "A survey of the Hough transform," *Computer vision, graphics, and image processing*, vol. 44, pp. 87-116, 1988.
- [30] Xu, L. and E. Oja, "Randomized Hough transform (RHT): basic mechanisms, algorithms, and computational complexities," *CVGIP: Image understanding*, vol. 57, pp. 131-154, 1993.
- [31] Penner, M.H., *Basic Principles of Spectroscopy*, Springer, 2010.
- [32] Urakawa, A., T. Bürgi, and A. Baiker, "Sensitivity enhancement and dynamic behavior analysis by modulation excitation spectroscopy: Principle and application in heterogeneous catalysis," *Chemical Engineering Science*, vol. 63, pp. 4902-4909, 2008.
- [33] HLETRD, "<http://teci.tistory.com/4>."
- [34] Point grey corp., "<https://www.ptgrey.com/>."
- [35] Edmundoptics corp, "<https://www.edmundoptics.co.kr/resources/application-notes/optics/optical-filters/>."
- [36] Semrock corp., "<https://www.semrock.com/>."
- [37] wiki, "https://en.wikipedia.org/wiki/Hough_transform."
- [38] Suard, F., et al. "Pedestrian detection using infrared images and histograms of oriented gradients," *in Intelligent Vehicles Symposium*, 2006.
- [39] Zhu, Q., et al., "Fast human detection using a cascade of histograms of oriented gradients," *in Computer Vision and Pattern Recognition*, IEEE Computer Society Conference on , 2006.
- [40] Dalal, N. and B. Triggs., "Histograms of oriented gradients for human detection," *in Computer Vision and Pattern Recognition*, IEEE Computer Society Conference on. 2005. IEEE.
- [41] S. Sural, G. Qian, and S. Pramanik, "Segmentation and histogram generation using the HSV color space for image retrieval," *in Image Processing. 2002. Proceedings, International Conference on*, vol. 2, pp. II-II, 2002

- [42] M. Abdullah-Al-Wadud, M. H. Kabir, M. A. A. Dewan, and O. Chae, "A dynamic histogram equalization for image contrast enhancement," *IEEE Transactions on Consumer Electronics*, vol. 53, no. 2, 2007.
- [43] T. Arici, S. Dikbas, and Y. Altunbasak, "A histogram modification framework and its application for image contrast enhancement," *IEEE Transactions on image processing*, vol. 18, no. 9, pp. 1921-1935, 2009.
- [44] H. Yoon, Y. Han, and H. Hahn, "Image contrast enhancement based sub-histogram equalization technique without over-equalization noise," *World Academy of Science, Engineering and Technology*, vol. 50, pp. 2009, 2009.
- [45] J. A. Stark, "Adaptive image contrast enhancement using generalizations of histogram equalization," *IEEE Transactions on image processing*, vol. 9, no. 5, pp. 889-896, 2000.
- [46] X. Ji, Y. Feng, G. Liu, M. Dai, and C. Yin, "Real-time defogging processing of aerial images," in *Wireless Communications Networking and Mobile Computing (WiCOM)*, 2010 6th International Conference on, 2010, pp. 1-4: IEEE.
- [47] P. Kumar, S. Henikoff, and P. C. Ng, "Predicting the effects of coding non-synonymous variants on protein function using the SIFT algorithm," *Nature protocols*, vol. 4, no. 7, pp. 1073-1081, 2009.
- [48] P. C. Ng and S. Henikoff, "SIFT: Predicting amino acid changes that affect protein function," *Nucleic acids research*, vol. 31, no. 13, pp. 3812-3814, 2003.
- [49] K. K. V. Toh and N. A. M. Isa, "Noise adaptive fuzzy switching median filter for salt-and-pepper noise reduction," *IEEE signal processing letters*, vol. 17, no. 3, pp. 281-284, 2010.
- [50] J.S. Lee, "Digital image smoothing and the sigma filter," *Computer vision, graphics, and image processing*, vol. 24, no. 2, pp. 255-269, 1983.

- [51] H. Seifarth et al., "Assessment of coronary artery stents using 16-slice MDCT angiography: evaluation of a dedicated reconstruction kernel and a noise reduction filter," *European radiology*, vol. 15, no. 4, pp. 721-726, 2005.
- [52] Z.Q. Yang, X.-Y. Wei, Z. Yi, and G. Friedland, "Contextual Noise Reduction for Domain Adaptive Near-Duplicate Retrieval on Merchandize Images," *IEEE Transactions on Image Processing*, 2017.
- [53] Y. Piao and H. Park, "Image resolution enhancement using inter-subband correlation in wavelet domain," in *Image Processing, IEEE International Conference on*, vol. 1, pp. I-445-I-448, 2007
- [54] S. S. Agaian, K. Panetta, and A. M. Grigoryan, "Transform-based image enhancement algorithms with performance measure," *IEEE Transactions on Image Processing*, vol. 10, no. 3, pp. 367-382, 2001.
- [55] R. Maini and H. Aggarwal, "A comprehensive review of image enhancement techniques," *arXiv preprint arXiv:1003.4053*, 2010.
- [56] J.S. Lee, "Digital image enhancement and noise filtering by use of local statistics," *IEEE transactions on pattern analysis and machine intelligence*, no. 2, pp. 165-168, 1980.
- [57] Wiki, "<https://en.wikipedia.org/wiki/Histogram>."
- [58] D. Young, "<http://www.cleanimages.com/article-understandingyourdigitalcamerashistogram.asp>."
- [59] L. Shao, J. Han, P. Kohli, and Z. Zhang, "Computer vision and machine learning with RGB-D.," sensors. *Springer*, 2014.
- [60] R. Jain, R. Kasturi, and B. G. Schunck, "Machine vision.," *McGraw-Hill New York*, 1995.
- [61] R. Hartley and A. Zisserman, "Multiple view geometry in computer vision.," *Cambridge university press*, 2003.
- [62] S. J. "Prince, Computer vision: models, learning, and inference.," *Cambridge University Press*, 2012.

- [63] scikit-image. "http://scikit-image.org/docs/stable/auto_examples/features_detection/plot_template.html."
- [64] G. J. Vanderbrug and A. Rosenfeld, "Two-stage template matching," *IEEE Transactions on Computers*, vol. 26, no. 4, pp. 384-393, 1977.
- [65] S. Pereira and T. Pun, "Robust template matching for affine resistant image watermarks," *IEEE transactions on image Processing*, vol. 9, no. 6, pp. 1123-1129, 2000.
- [66] Y. Lee, T. Hara, H. Fujita, S. Itoh, and T. Ishigaki, "Automated detection of pulmonary nodules in helical CT images based on an improved template-matching technique," *IEEE Transactions on medical imaging*, vol. 20, no. 7, pp. 595-604, 2001.

감 사 의 글

대전으로 내려와서 지내온 날에 비한 짧은 기간동안 많은 것을 느끼게 해준 감사한 사람들이 너무 많습니다. 저의 연구에 항상 많은 도움을 주시고, 때로는 엄격한 교수님으로써 때로는 존경스러운 인생의 선배로써 항상 저를 가르쳐주신 존경하는 김경수 교수님께 감사의 말씀 전하고 싶습니다. 교수님의 학문적인 가르침은 이제는 받기 어렵겠지만, 교수님의 다른 사람을 배려하시고 웃사람을 공경하시고 그리고 낮은 사람에게 배푸시는 마음은 저를 이루는 큰 인성 철학의 축으로 오랜 기간 저를 지탱할 것 같습니다. 감사합니다.

우리 연구실은 사람이 너무 많아 서로 서운한 점도 생길 법도 한데 서로 모난 모습없이 행복하게 잘 사는 것 같습니다. 내 룸메이트로 항상 나에게 자극이 되어준 영진이형, 지금은 졸업하고 없지만 같은 기간에 연구실에 들어와서 동거동락했던 운태형, 동현이형. 기가막힌 아이디어와 못하는게 없는 흰칠한 솜씨로 15년 겨울바람을 새차게 맞은 저를 졸업하게 도와준 민영이형, 항상 내옆에서 정말 친한 친구처럼 말동무와 훌륭한 게임 파트너가 되어준 성준이형, 우용이형. 고개를 들어 맞은 편을 바라보면 항상 같은 표정 같은 자세로 연구하는 생각보다 빨간남자 경환이형, 나도 잘 못하는데 맨날 내 잔소리 다 들어주고 내 장난 다 받아준 병철이형.

이제는 구신랑 치웅이형, 전력전자 회로왕 용훈이형, EPS의 아버지이며 유일한 비트의 수혜자 동욱이형, 섹시 쿨가이 형태형, 손동이 병관이형, 영원할 줄만 알았던 대쪽같던 금육선비 대현이형까지 같은 공간에서 생활하면서 시끄럽고 헛소리 많이 하는 동생한테 잔소리 한번은 안해준 형들, 그리고 언제나 만나면 신세한탄 헛소리 뿐인 게임왕 영걸이형, 킹 오브 더 둔산 동현이, 화가나면 무서울 것 같은 재환이, 솔직해서 너무 좋은 우리 진우, 늦게 들어온 미림누나까지 모두 감사합니다. 인생의 선배로 저의 고민을 많이 들어준 주원이형, 연구 많이 도와준 승렬이형, 연구실의 역사를 알게해준 민구형, 아우라로 덮혀있어 항상 다가가기 어려운 상우 외에도 문지에 있으면서 많이 같이 생활하지 못했던 MSC 식구들 너무 감사합니다.

이제는 대부분 사회로 나가서 어렵고 힘든 시기를 같이 보내는 만큼 서로에게 더 의지하고 더 놀릴 수 있는 채휘병, 윤서진, 우령찬, 이용진, 임채원. 나의 고등학교 동창들 앞으로도 지금처럼 일년에 두번씩만이라도 만나서 헛소리하면서 웃고 떠들고 즐길 수 있는 사이면 좋겠습니다. 그리고 경식, 동운, 호준, 주현, 미림, 수연, 수정, 석진, 아란, 은샘, 진웅, 해원, 솔지등 대학교 동창들, 헤리, 종원 등 동아리 친구들. 서로

어렵고 힘든 시기인데도 저를 붙잡고 때로는 처음 만났을 때처럼 놀리고 놀리면서 같은 모습 그래도 있어 주어서 너무 감사합니다.

제가 석사기간동안 우리 가족에게는 많은 변화가 있었습니다. 때로는 가슴아프게 슬프기도 때로는 눈물나게 기쁜일도 있었습니다. 그래서인지 이 짧은 2년이라는 기간이 저에게는 너무 크게 다가오는 것 같습니다. 지금은 많이 편찮으신 우리 할머니, 막내 손자 올때마다 안아주고 반겨줘서 너무 고맙습니다. 누구보다 힘든 시기에 내색하지 않고 가장의 무게를 지키며 가족들을 위해 개인을 희생해온 아버지. 항상 우리 형제들의 우상이었던 모습 그대로 있어주셔서 너무 감사합니다. 우리 가족만을 바라보며 집에가면 언제나 밝은 미소로 반겨주는, 때로는 소녀같은 우리 엄마도 너무 고맙습니다. 이젠 곧 어엿한 아빠가 되는 우리 형, 우리 가족에게 너무 큰 선물인 우리 소영형수 그리고 내 조카 차차도 정말 감사합니다.

그동안 기동만 같았던 아버지의 우직함이, 그저 한결같은 줄만 알았던 엄마의 미소가 2년이라는 짧은 시간 동안 아버지의 우직함이 얼마나 어려운지, 엄마의 미소가 때로는 여리게 느껴지게 됐습니다. 우리 가족의 존재를 당연하다고 느껴 소중함이 있고 나만 바라보며 살았었는데, 최근 2년동안 내적으로 외적으로 힘든 일을 많이 겪으면서 가족의 소중함이라는 매길 수 없는 가치에 대해서 많이 진정으로 깨닫게 됐습니다. 이 기회를 빌어서 감사하다고 사랑한다고 전하고 싶습니다.

그리고 항상 내 옆에서 때로는 웃음도 투정도 장난도 애교도 많이 부려준, 무엇보다 가족이라는 소중한 존재에 대해서 많이 깨닫게 해준 사랑하는 내 여자친구 지현이에게도 고맙습니다. 앞으로도 지금처럼 서로의 곁에서 의지하고 성장하며 좋은 일만 가득했음 좋겠습니다.

약 력

이 름: 조 정 석

생 년 월 일: 1993년 08월 30일

출 생 지: 서울특별시

주 소: 경기도 양주시 천보산로 100번길 119

전 자 주 소: cjs3178@gmail.com / jscho7178@kaist.ac.kr

학 력

2009. 3. - 2012. 2. 의정부고등학교

2012. 3. - 2015. 8. 인하대학교 전자공학과 (학사)

연구 업 적

1. J. Cho, J. Park U. Back et al., "Automatic Parking System using Background Subtraction with CCTV Environment", *2016 16th International Conference on Control, Automation and Systems (ICCAS)*, Gyeongju, 2016, pp. 1649-1652.
2. M. Lee, K. S. Kim, J. Cho and S. Kim, "Development of a vehicle body velocity sensor using Modulated Motion Blur," *2017 IEEE International Conference on Advanced Intelligent Mechatronics (AIM)*, Munich, 2017, pp. 406-411.